2011-03-09

Time-series Observations of the High Mass X-Ray Binary 4U 2206+54 to Monitor Light Variation

Jessica Lynn Bugno
Brigham Young University - Provo

Time-series and Multifilter Analysis of the High Mass X-ray Binary 4U 2206+54 to Monitor Light Variation

Jessica L. Bugno

A thesis submitted to the faculty of
Brigham Young University
in partial fulfillment of the requirements for the degree of

Master of Science

Eric G. Hintz, Chair
Victor Migenes
Denise C. Stephens

Department of Physics and Astronomy

Brigham Young University

April 2011

ABSTRACT

Time-series and Multifilter Analysis of the High Mass X-ray
Binary 4U 2206+54 to Monitor Light Variation

Jessica L. Bugno
Department of Physics and Astronomy
Master of Science

The high mass X-ray binary 4U 2206+54 has been a very controversial system due to variability in spectral data as well as photometric data. We, at Brigham Young University, have been observing this system in multiple filters with several telescopes. This thesis presents our methods of observations, reductions, and results. It also compares what we have been detecting to other groups looking at the same target in different wavelengths. Furthermore, this thesis discusses some of the peculiarities of 4U 2206+54 and possible theories to explain these phenomena. Based on our photometric observations for the past three years, we believe the period of 4U 2206+54 is 25.1 days. Furthermore, spectral data show an unusual double-peaked $H\alpha$ feature. We believe the primary star BD +53°2790 is a single star, and that the system is surrounded by a gas and dust shell.

Keywords: 4U 2206+54, BD +53°2790, high mass x-ray binaries, accretion, reduction methods, standardization, δ Scuti

ACKNOWLEDGMENTS

There are many people who played a great role in helping me with my project and throughout my time at Brigham Young University. Dr. Eric Hintz, my advisor, has guided me through not only the observational techniques, but also the data reduction. Both of these areas were completely new to me when I first arrived. Prof. Michael Joner and Dr. David Laney have provided me with their help and knowledge working at West Mountain Observatory. Dr. Victor Migenes has opened my eyes to the world of radio astronomy, and has also been there for advice for my graduate studies. Last, but not least, I would like to thank my family and friends who have always been there for me, and have kept me going through the darkest of times. These influential people have made it possible for my time at BYU to be a success.

Contents

List of Figures

Chapter 1

Introduction and Background

1.1 High Mass X-ray Binaries

This project was designed to observe the high mass X-ray binary (HMXB) 4U 2206+54 at multiple wavelengths to determine the orbital period of the system. Several periods have already been published, but we believe that these are incorrect. Using our own time series and multifilter analysis, we plan to refine the orbital period.

HMXBs consist of a massive star, normally an O or B type star, and either a neutron star or black hole. The massive star can make HMXBs easier to observe than low mass X-ray binaries (LMXBs) because HMXBs are brighter in both optical and X-ray wavelengths. LMXBs tend to have apparent magnitudes in the upper teens, while HMXBs have typical apparent magnitudes in single digits or lower teens. In both cases, the compact object rips matter away from the massive star, thus creating the X-rays. The high mass primary star distinguishes the HMXBs from the LMXBs (Sarty et al. 2007).

The “high mass" in HMXB refers to the O or B star. It is true, however, that the compact companion was formed from a more massive star. The original more massive star fused hydrogen

to helium in its core much more rapidly than its companion, and had a relatively short lifetime on the main sequence. Based on the standard model of stellar evolution, stars leave the main sequence when hydrogen to helium fusion stops *in the core*. H→He fusion can still occur in the layers of the star just outside the core. This makes the gas expand and cool, which causes the star to become a red giant. Fusion processes in the outer layers create helium ash, which "rains" down onto the core. For high mass stars, the temperature in the core gradually increases until fusion of helium into carbon begins. Massive stars will repeat a similar process creating heavier elements down to iron. This causes several shells to be fusing simultaneously making the star expand to become a supergiant (Kippenhahn & Weigert 1990).

Fusion continues until iron is formed in the core. At this point, temperatures are not sufficient to fuse the iron, so the core shrinks since there is no more outward pressure due to thermonuclear reactions. The outer layers begin to fall towards the core, but since the core is extremely dense, $\rho \geq 10^{14}$ kg/m^3, the infalling material rebounds off the compact core with a velocity greater than the speed of sound. This produces a shock wave that carries the outermost layers of the star away. This event is known as a core-collapse supernova. The leftover core from the original star will be a neutron star. If the mass of the original star is great enough ($M > 8$ M$_\odot$), a black hole may be left behind instead (Kippenhahn & Weigert 1990). This compact leftover is half of the HMXB system.

It is possible that if the O or B type star in the HMXB is at apastron, its orbit would not be affected by the supernova. Another possibility is the O or B type star could have formed from a pocket of gas from the supernova, and will now orbit the compact object.

HMXBs come in two classes: short orbital period and long orbital period. Short periods are typically a couple of days, while long periods can be weeks to years. Short period binaries can have matter continually passing from the high mass star to the neutron star or black hole. The long period binaries differ in that when the star is at its apastron distance, it is far enough away that mass is not directly pulled off by the companion, leading to a decrease in the X-ray intensity due

to the absence of interaction (Sarty et al. 2007).

Finding the period of a binary system is extremely valuable because it allows the researcher to determine the separation between the two objects. Kepler's Third Law can be expressed as the following:

$$a = 5(M_1 + M_2)^{1/3} P^{2/3} \tag{1.1}$$

where a is the separation in $R_\odot$, both masses in $M_\odot$, and P is in days. Equation 1.1 can be used if the masses are known, if not exactly, then at least approximately (Charles & Seward 1995). If the separation is already known, Equation 1.1 can be used to determine the two masses instead.

There are, however, some interesting complications with observing HMXBs. When analyzing the light curve for interactions between the two objects, it is possible to see very rapid changes in brightness, which is sometimes referred to as a wiggle. Normally this is a sign that there has been an interaction, but there is also the potential that this wiggle is caused by the O or B companion pulsating. This effect happens for short period orbits because the two objects are so close together (Sarty et al. 2007).

Another complication is when the B star, typically 8 to 15 $M_\odot$, is pulsating very rapidly. When this occurs, the massive star can develop an equatorial disk where mass can be lost. This gives off emission spectra, which can make it difficult to specify the spectral type of this star. This can be observed for long period orbits because there is not a continual transfer of matter due to the greater distance of the orbit (Sarty et al. 2007).

A third complication depends on how much mass the black hole or neutron star receives from its partner. If it is only a small fraction of the overall mass of the O or B star, there is not much effect on the orbit of that star. However, if a significant amount of mass is taken, then this could change the eccentricity of the orbit. A change in orbit can also be caused when one partner in the binary initially goes supernova. The force from the explosion will send out a shockwave which may or may not alter the path that the other star takes. Even though there may be another compact

object left behind from the supernova, the binary will not exist anymore due to the shockwave disturbing the primary star if it is nearby. If the shockwave does not force the partner far enough away, which is possible when the primary star is at apastron in a long period orbit, there will be a new high mass X-ray binary formed (Sarty et al. 2007). Changes in the orbit will make the orbital period much more difficult to determine.

1.2 Accretion onto the Compact Object

The amount of material accreted by the compact object from the stellar wind of the "normal" star can be determined using the Bondi-Hoyle method. There are three main assumptions for this method: the stellar wind itself is uniform, the stellar wind is moving from the surface of the "normal" star uniformly in all directions, and the orbit of the massive star is circular or nearly circular. Not all of the wind will accrete onto the compact object. This is taken into account by creating an accretion cylinder, as seen in Figure 1.1. The cylinder has a radius, r_{acc}, and only material that is within this radius will accrete onto the compact object. Material just outside this radius will be perturbed from its path, but will not accrete. This forms an accretion wake around the compact object (Charles & Seward 1995). The accretion radius can be calculated as follows:

$$r_{acc} = \frac{2GM_x}{v_{rel}^2} \tag{1.2}$$

Here, v_{rel}^2 is the relative velocity between the stellar wind, v_w, and the motion of the compact object, v. M_x is the mass of the compact object. The relative velocity can be found by:

$$v^2 = \frac{GM_n}{a} \tag{1.3a}$$

$$v_{rel}^2 = v^2 + v_w^2 \tag{1.3b}$$

where M_n is the mass of the "normal" star, and a is the radius of the orbit. Only the material that enters the accretion cylinder will accrete onto the compact object, so the mass flow rate, or the

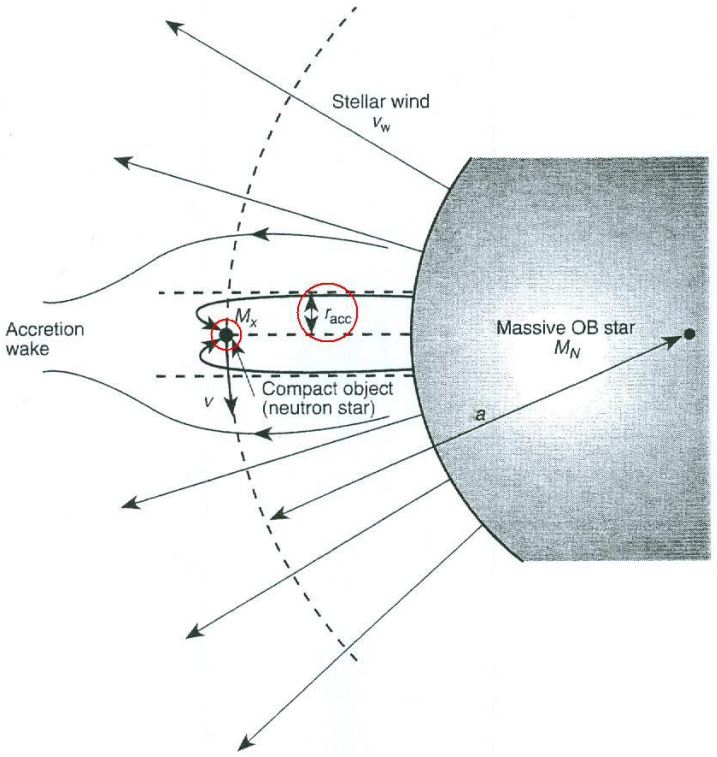

Figure 1.1 Diagram of the accretion cylinder in an HMXB (Charles & Seward 1995)

amount of mass that passes through a given area, is given by the following:

$$\dot{M} = \pi r_{acc}^2 v_{rel} \rho \tag{1.4}$$

where ρ is the density of the stellar wind given by Equation 1.5:

$$\rho = \frac{M_w}{4\pi a^2 v_w} \tag{1.5}$$

and M_w is the total mass loss due to stellar winds. Now it is possible to determine the fraction of stellar wind that is accreted by the compact object by rearranging the previous equations:

$$\frac{\dot{M}}{\dot{M}_w} = \left(\frac{M_x}{M_n}\right)^2 \frac{\left(\frac{v}{v_w}\right)^4}{\left[1+\left(\frac{v}{v_w}\right)^2\right]^{3/2}} \tag{1.6}$$

1.3 The HMXB 4U 2206+54

1.3.1 General Information on 4U 2206+54

Our focus is the HMXB LPH 128, also known as 4U 2206+54. The main goal of this project is to identify and refine the orbital period of this particular HMXB. From the literature, the period was originally determined to be 9.6 days (Corbet & Peele 2001) using data from Rossi X-Ray Timing Explorer (RXTE) (Levine et al. 1996). But after analyzing observations from the Swift Burst Alert Telescope (Barthelmy et al. 2005), a period of 19.25 $\pm$ 0.08 days (Corbet et al. 2007) is found, almost exactly double what the RXTE determined. It is suspicious that the second value is a multiple of the first. It is possible that there is a mistake in the analyses, or the difference in these measurements could occur because of the uncertain nature of the high mass companion. It is possible that the high mass star has an equatorial circumstellar disk, depending on what spectral type it is. The compact companion could pass through this disk and create peaks in the luminosity (Corbet et al. 2007). The actual reason for this difference is not yet clear.

1.3.2 The Massive Companion of 4U 2206+54, BD +53°2790

There is a discrepancy in the spectral classification for the high mass companion, BD +53°2790. There have been arguments to suggest that this star is a Be star (Steiner et al. 1984), where the "e" represents emission. However, there are other arguments that suggest it is an O-type star. Both arguments were based on observations of the Hα line in the star's spectrum (Corbet et al. 2007).

According to Steiner et al. (1984), BD +53°2790 was estimated to be a B0-2e main sequence star, based on photometric observations. The system was therefore classified as a Be/X-ray binary because the Classical X-ray Binaries have supergiants as the OB companion. The spectrum of BD +53°2790 also displayed strong O II and Si III triplet absorption lines, both commonly found in the spectrum of an early B-type star (Negueruela & Reig 2001). See Figure 1.2 for a graphical

representation of the strength of absorption lines as a function of surface temperature and spectral type. Based on July 1995 optical spectroscopy observations, these two lines were strong and clearly visible. In August 1998 observations, the lines were almost too weak to see. July 2000 observations captured the two lines again, but this time the intensity detected was approximately the average intensity of the two extremes (Negueruela & Reig 2001). In later years, a strong He

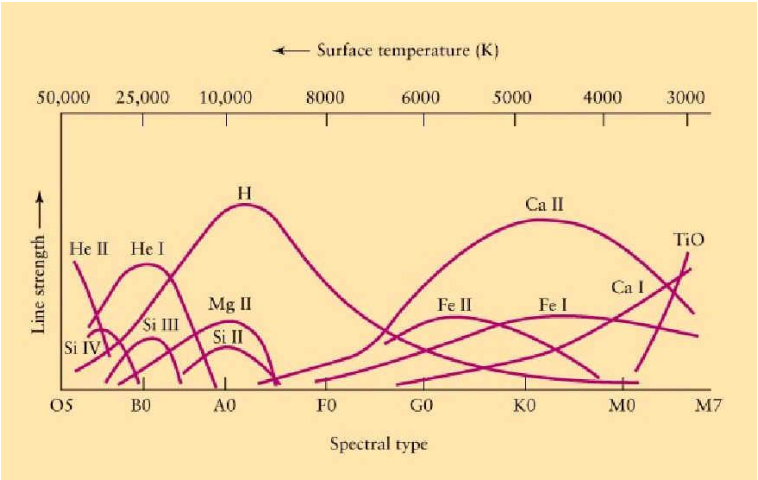

Figure 1.2 This graph shows the strength of absorption lines for different surface temperatures (Freedman & Kauffman 2008).

II absorption line was observed by P. Blay, which is a characteristic of an O-type star (Blay et al. 2006). An O-type star exhibits this feature, as seen in Figure 1.2, because the surface temperature is much higher and therefore able to ionize helium. BD $+53°2790$ is still believed to be on the main sequence (Reig et al. 2009). Furthermore, the ultraviolet spectroscopy commented on in Negueruela & Reig (2001) is best matched to a late OV star. See Table 1.1 for more information about main sequence lifetimes and color indices. It is possible that the confusion about the spectral type is due to the variable spectrum of the star.

Complications also arise when observing in Hα. As seen in Blay et al. (2006), there is strong

Table 1.1. Main Sequence Lifetimes and Color Indices for Different Spectral Types

Spectral Type	Teff (K)	MS Lifetime (Myrs)	B - V	V - R	R - I
O5	47,000	3.80	-0.32	···	···
O7	38,000	6.76	-0.32	···	···
B0	30,500	12.03	-0.30	-0.19	0.11
B5	15,000	31.42	-0.16	-0.10	0.06
A0	9500	82.06	0.00	-0.04	-0.04
A5	8300	214.33	0.15	0.04	-0.11
F0	7300	559.76	0.29	0.12	-0.17
F5	6600	1461.93	0.42	0.21	-0.21
G0	5900	3818.11	0.58	0.27	-0.31
G5	5600	9971.74	0.69	0.31	-0.38
K0	5100	26,043.16	0.85	0.42	-0.43
K5	4200	68,016.84	1.16	0.68	-0.48
M0	3700	177,639.33	1.42	0.70	-0.72
M5	3000	463,940.02	1.61	···	···

References. — (Freedman & Kauffman 2008), (Mihalas et al. 1981), (Reid 2010)

Hα emission that is believed to come from BD +53°2790. However, the emission peak is actually broken by an absorption trough. Looking at the left portion of Figure 1.3 taken from Blay et al. (2006), beginning on May 28, 1986 one can see a variation in the strength of the emission peaks as time progresses. Sometimes the absorption trough passes below the continuum level, and other

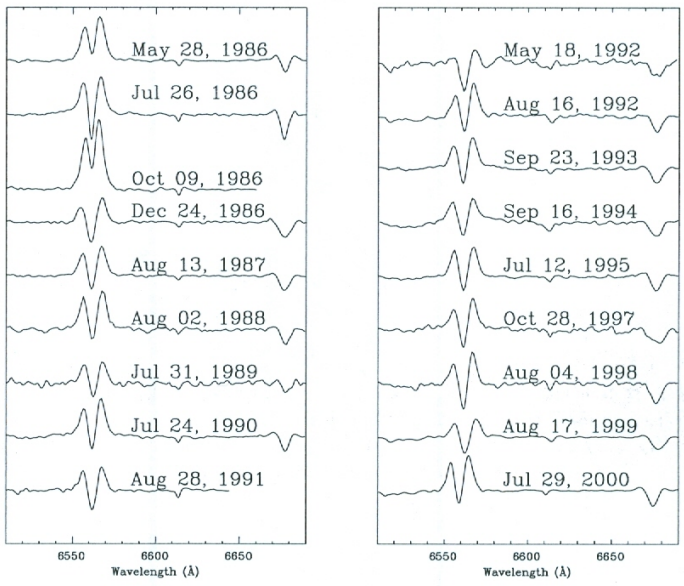

Figure 1.3 Hα observations of BD +53°2790 (Blay et al. 2006)

times not even reaching that level. In the right portion of the same figure, it is clear that the emission peaks have varied in amplitude by 20-80%. The cause of these amplitude changes is still uncertain.

Negueruela & Reig (2001) provide suggestions as to what the nature of BD +53°2790 might be based on the changing spectral line intensities. One possibility is that BD +53°2790 is part of a spectroscopic binary, which therefore means 4U 2206+54 is a binary system within a binary system. Even though this does seem quite complicated, if BD +53°2790 is a late O-type star partnered with an early B-type star, then when the B star passes in front of the O star, spectral lines

would appear to be those common to a B-type star, like the O II line. Similarly, when the O star is in front, spectral lines will resemble those of this spectral type, like He II, and weak O II and Si III lines. It is still necessary to have the compact companion in 4U 2206+54 to produce the hard X-rays from wind accretion (Negueruela & Reig 2001).

Another obvious suggestion is that BD $+53°2790$ is a peculiar star that has some physical mechanism unknown to astronomers at this point (Negueruela & Reig 2001).

An additional discrepancy is the relationship between the equilibrium width (EW) of the He I line and the EW of the Hα line. Blay et al. (2006) has noted that there is some degree of correlation between these two lines, as depicted in Figure 1.4. However, looking at the statistical analysis of the correlation, it is not strong at all. The line of best fit was drawn through the data points, but the data do not seem to be linear. In particular, there are two outliers. The reason for these has not been determined. Some other data points are also a fair distance away from the best fit line. Therefore, looking at the plot as a whole, there does not seem to be much of a correlation.

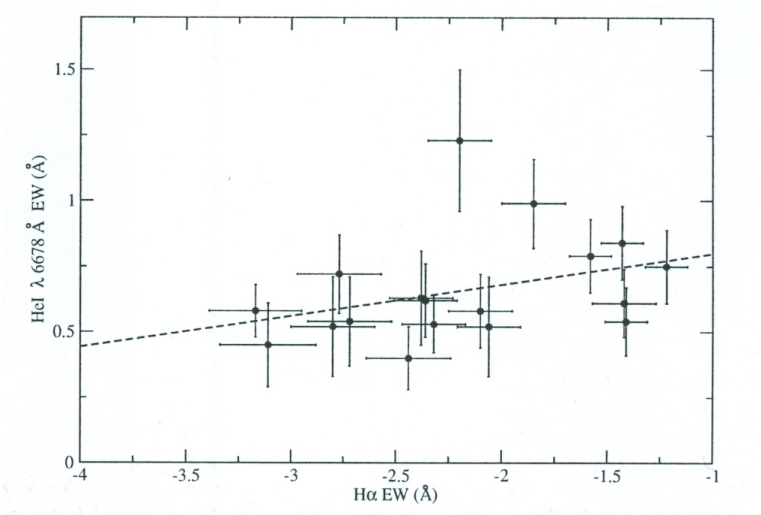

Figure 1.4 Correlation between the EW of the Hα line (x-axis) and the EW of the He I line (y-axis). The regression correlation coefficient is $r = 0.62$ (Blay et al. 2006).

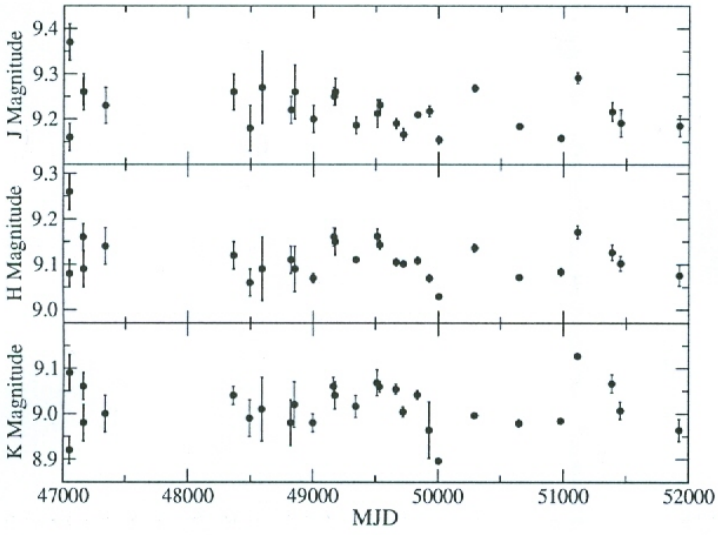

Figure 1.5 IR observations of BD $+53°2790$ (Blay et al. 2006)

Observations were also taken in infrared (IR) by P. Blay. According to Blay et al. (2006), there was no significant long-term variability seen, with an approximate magnitude range of 0.2 mag in the J, H, and K bands, as seen in Figure 1.5. It does seem, however, that small variations of approximately 0.12-0.22 mag do occur in all three bands. Blay et al. (2006) also discusses spectroscopic findings. See Section 2.2.1 for further details.

1.3.3 Peculiarities of 4U 2206+54

Another peculiarity of 4U 2206+54 is the complete lack of X-ray pulsations, as the majority of HMXBs behave similarly to an X-ray pulsar. However, the variability of 4U 2206+54 does not show this behavior. It is believed that the system's variability is caused by wind accretion onto the compact object. A problem with this theory is that most wind-fed systems observed to date have an X-ray pulsar as a compact companion, which would have well defined X-ray pulsations (Blay et al. 2005). This could be explained by co-aligned magnetic and rotational axes of the neutron

star. Another explanation is a neutron star companion with a low magnetic field.

The compact object is believed to be a neutron star or black hole. Even though the black hole would explain some of the uncertainties about the system, the X-ray spectrum matches the neutron star model more closely (Corbet & Peele 2001).

However, these models do not explain why 4U 2206+54 has an unusually low X-ray luminosity for an HMXB. One process that can account for low X-ray luminosity is accretion onto the neutron star by the stellar wind from the high mass star. Since the high mass star is believed to be a main sequence star and not a supergiant, the stellar wind should be rather weak, approximately $3 \cdot 10^{-8} M_{\odot}$ yr^{-1} or less. According to Ribó et al. (2006), the calculated wind terminal velocity for BD $+53°2790$ ($v \approx 350$ km s^{-1}) is also slower than the established wind terminal velocity for O9V stars, which range from 1120-1925 km s^{-1}. This, however, does not explain the lack of X-ray pulsations (Corbet & Peele 2001).

Additional evidence suggests that BD $+53°2790$ is not a Be-type star, but rather an O-type star. The expected X-ray luminosity for an O9V star is $\sim 10^{34}$ erg s^{-1}. But the detected X-ray luminosity coming from 4U 2206+54 is $\sim 10^{35} - 10^{36}$ erg s^{-1}. Furthermore, according to Blay et al. (2005), the semi-major axis of this system is 55-60$R_{\odot}$, which may account for the low X-ray luminosity due to a larger distance.

1.4 The δ Scuti GSC 03973-01698

A δ Scuti variable star is a star that undergoes periodic, typically on the order of hours, or sometimes aperiodic changes in its brightness. These changes are due to expansion and contraction of the star. This pulsation can be adiabatic radial, non-adiabatic radial, or non-radial. Adiabatic radial pulsations are uniform pulsations of the star, meaning the outer layers expand and contract together, with no energy transfer or heat change during the movement. Somewhat more realistic

is the non-adiabatic radial motion because the movement of the gas will produce heat flow. Non-radial refers to pulsations that are not symmetric about the star. Determining the type of pulsational mode can be challenging, especially if the star is rotating (Kippenhahn & Weigert 1990).

We were very fortunate to have a δ Scuti variable star, GSC 03973-01698, in the same field as 4U 2206+54. The locations for these objects are marked in Figure 1.6. This is helpful because the

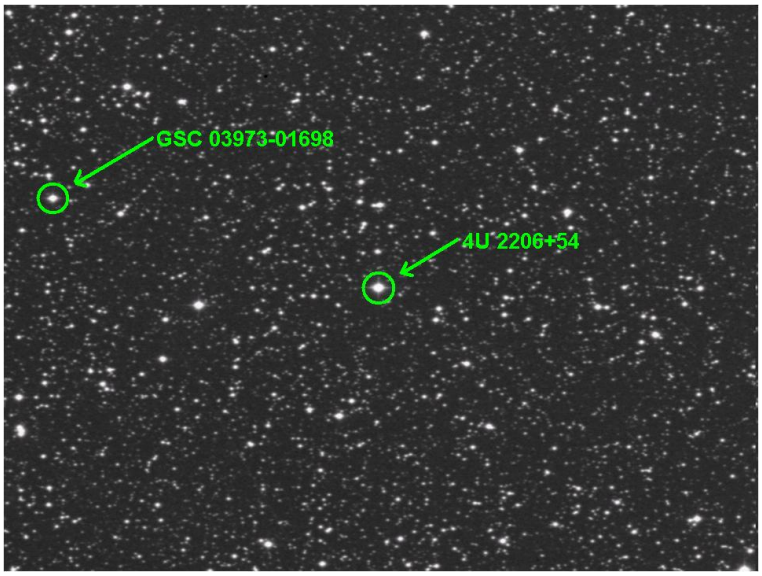

Figure 1.6 This is the starfield for 4U 2206+54.

lightcurve for a δ Scuti is a sinusoidal shape, as seen in Figure 1.7. Because of this, we know if the lightcurve for the δ Scuti in the field has a distinct wave pattern, the data for 4U 2206+54 have been processed correctly. If there is no wave pattern, then the variation detected for 4U 2206+54 would be questionable. Fortunately, this was not the case. For a more extensive look at GSC 03973-01698 see Hintz et al. (2009).

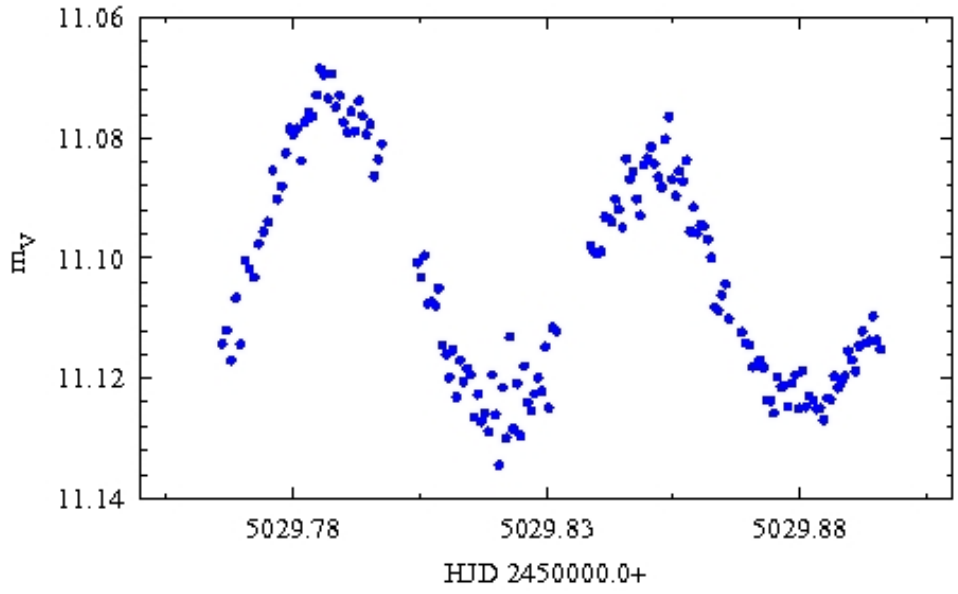

Figure 1.7 This is a lightcurve of GSC 03973-01698 from July 17, 2009, taken at the Orson Pratt Observatory.

Chapter 2

Observations

2.1 Photometric Observations

Photometric observations of 4U 2206+54 were taken during the summers of 2008, 2009, and 2010. The David Derrick Telecope (DDT) in the Orson Pratt Observatory (OPO) was used to obtain photometric data with the Johnson *BVRI* filters. Three additional telescopes were used at the West Mountain Observatory (WMO): the 0.32 m, the 0.51 m, and the 0.9 m.

2.1.1 Orson Pratt Observatory

At the OPO, the DDT (Figure 2.1) was used for all observations. The DDT is a 0.41 m reflecting telescope with a 31' x 21' field of view. During 2008 and 2009, the Newtonian focus was used, which has a focal ratio of $f/4$. The CCD used at that time was an ST-10 with a platescale of 0.864"/pixel. The only filter used with this CCD was the Johnson V, and the average CCD temperature during the summer was approximately -10° C.

In May 2010, an STL-1001 CCD was installed at the Cassegrain focus of the DDT, with a focal ratio of $f/12.5$. Around the same time, replacement filters were also installed. This made it

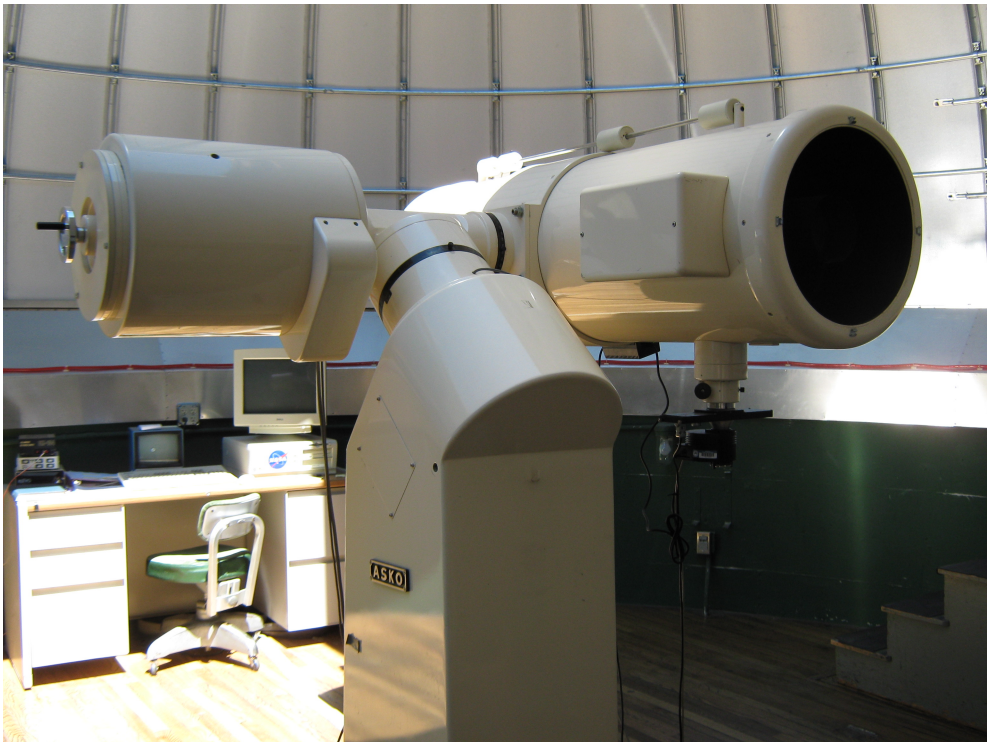

Figure 2.1 David Derrick Telescope.

possible to observe the field of 4U 2206+54 using the Johnson *BVI* filters. The average temperature of the CCD was -10° C during the summer.

2.1.2 West Mountain Observatory

During the summer of 2008, the 0.32 m reflecting telescope at WMO (Figure 2.2) captured images of 4U 2206+54 from July 8-11. The CCD installed on this telescope is an STL-1001, which gives rise to a 29.5'x29.5' field of view. The 0.32 m telescope has an $f/9$ focal ratio. There were also two days, July 2-3, where the 0.51 m reflecting telescope was used. The 0.51 m telescope also has an STL-1001 CCD, with a field of view of 20.5'x20.5' and a focal ratio of $f/8.1$. Both telescopes used the *V* filter.

Figure 2.2 West Mountain Observatory

For 2009, the 0.32 m and the 0.51 m telescopes were used again, for a total of 14 nights of observations. Again, only V filter data were taken.

A new addition to WMO is the 0.9 m telescope, which was installed during the summer of 2009. A PL9000 CCD produces a field of view of 25.1'x25.1' and the telescope has an $f/5.5$ focal ratio. The 0.9 m was only used for this project on September 26, 2010 for standard star observations. Secondary standards were later determined for other nights and years.

For 2010, we decided to perform a multifilter analysis on 4U 2206+54, so $BVRI$ images were taken using the 0.51 m telescope. A palindrome-like sequence was used, meaning $BVRI\ BVRI$ instead of $BVRI\ IRVB$, due to the operational software.

It is best to use several observatories and compare the results. This way light variation cannot

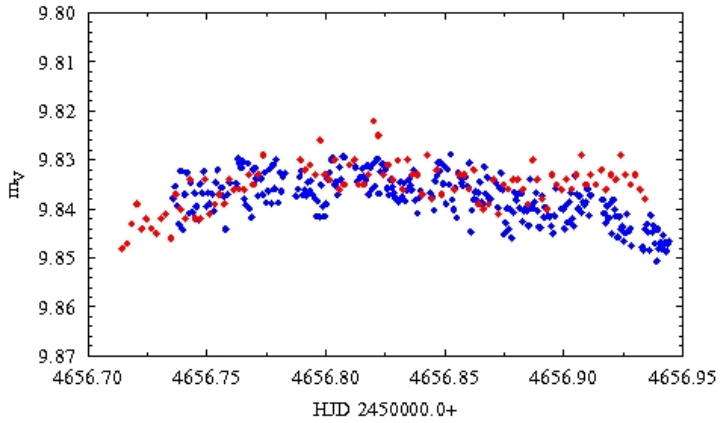

(a) 4U 2206+54

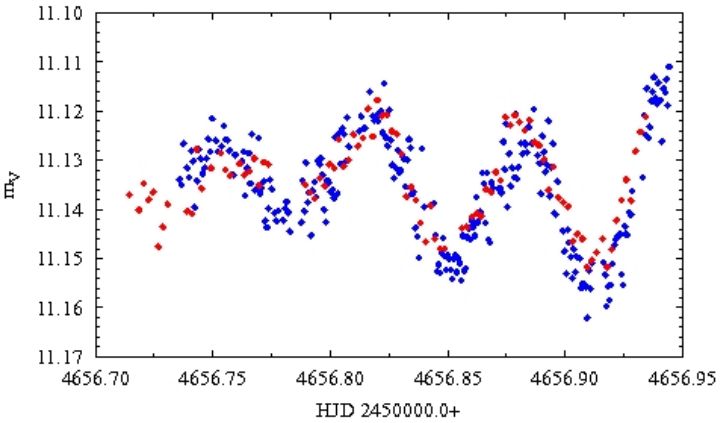

(b) GSC 03973-01698

Figure 2.3 Comparison graphs of the West Mountain Observatory (red) and Orson Pratt Observatory (blue) for 4U 2206+54 and GSC 03973-01698

be attributed to something in the mechanics of a single telescope. Having access to both OPO and WMO has given us such an opportunity. We have compared the data taken on July 9, 2008 at the OPO and WMO for 4U 2206+54 and GSC 03973-01698 as seen in Figure 2.3. The WMO observations bracket the OPO observations and throughout the night both sets of data stay almost completely aligned with each other.

2.2 Spectroscopic Observations

2.2.1 Dominion Astrophysical Observatory

At the Dominion Astrophysical Observatory (DAO) (Figure 2.4), we used the 1.2 m telescope and McKellar spectrograph, mounted at the Coudé focus. A 3231 grating with 300 grooves/mm and blazed at 4200 Å was used, which yields a dispersion of 41 Å/mm. The CCD was a SITe4, which has 15 micron pixels and gives rise to a resolution of 0.615 Å/pixel. These observations were used to observe the $H\alpha$ and $H\beta$ spectral lines. The nights received were July 31, August 1, and August 2 of 2009, as well as September 22, 2010. Each night had three frames.

Figure 2.4 The 1.2 m telescope at DAO

2.2.2 Observatorio el Roque de los Muchachos

Other spectroscopic observations of 4U 2206+54 were taken for P. Blay at the Observatorio del Roque de los Muchachos in La Palma, Spain. This research took place on select nights from 1986 to 2000. The importance of this study is discussed in further detail in Section 4.2.2.

2.3 Radio Observations

The Very Large Array (VLA) observations of 4U 2206+54 were taken in May 2003 by P. Blay and in June 2008 by M. Ribó. However, these data were not sufficient for this project. For more information on the implications of the Ribó data and why radio observations are important, see Section 6.2.3.

Chapter 3

Analysis

3.1 Reduction Methods

The data collected from the telescopes are only raw data, and therefore must be processed before being analyzed. Because the CCD's are not perfect instruments, data reduction begins with three calibrations frames that are taken each night for each telescope. These frames are zeros (or bias), darks, and flats.

Photons from the source excite electrons in the wells of the chip of the CCD. The computer then reads the number of excited electrons as "counts." The zeros and darks are thermal corrections. These are necessary because stray electrons that have nothing to do with the source can be counted. This would give false readings if we did not know how many electrons are due to the source and how many are due to the electronics of the system. A zero frame is a zero second exposure that accounts for residual electrons. A dark frame is taken for at least the approximate exposure time as the source, but with the shutter closed. This accounts for "dark current," which is the current running through the instrument while taking a frame. Lastly, a flat frame is a light frame taken of a uniform field, usually the uniform blue sky at dusk or dawn. It can also be taken inside the

dome if the dome is uniform or if there is a screen and a light source, but this is not as common. The flat frame is necessary because the pixels in the chip do not respond equally to the incoming light. Since the field where the flats are taken is uniform, the differences in the pixel responsiveness can be detected. Due to the fact that a flat varies with wavelength, there must be a flat taken in each filter that will be used for source observations. Dark and zero frames do not require this. An example of raw and processed frames is shown in Figure 3.1.

Before the calibration frames can be applied, the headers, or list of information about the file, for the object frames need to be changed. The header includes such information as the telescope used, the CCD used, and the exposure time. However, this is incomplete. Knowing the coordinates of the object, the Heliocentric Julian Date (HJD) of each observation, the airmass, and the filter are also important. Using the image and Reduction and Analysis Facility (IRAF), there are two processes that can adjust the headers. One is applying a *.cmds* file. This file contains the right ascension, declination, filter, epoch, observatory, observer, type of image (in this case object), and the time zone of the sidereal time. To apply this file to the image headers, use the command *asthedit filename*.fits filename.cmds*, where the * will include all files with the root name *filename*. Next, the commands *setjd filename*.fits* and *setairmass filename*.fits* add the time and calculated airmass values, respectively, for each frame in the respective header by using the information provided in the *.cmds* file. See Figure 3.2 and Figure 3.3 for before and after examples of an object frame header.

Now in IRAF, the headers for the zero, dark, and flat frames must be adjusted. For this, we use the command *hedit filename*.fits imagetyp type*. For example, the zero line would look like *hedit zero*.fits imagetyp zero*. See Figure 3.4 for an example of a zero frame header.

The zero frames can then be combined using *zerocombine*. This will create a master zero frame. Next, a similar header adjustment must be made for the dark frames. After this, the master zero frame is applied to the dark frames. Then the darks can be combined to form the dark master

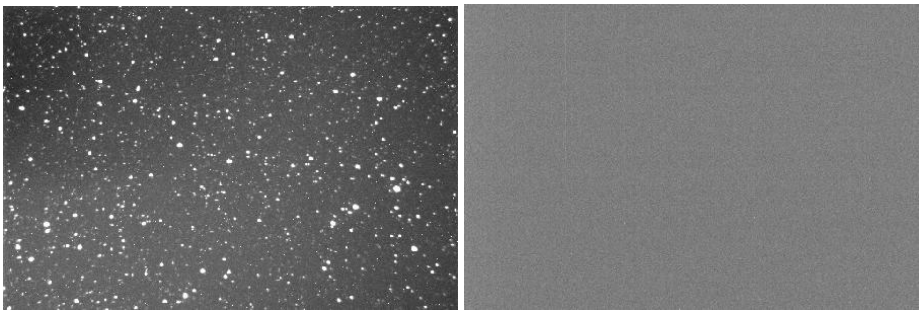

(a) Object frame before processing (b) Zero calibration frame

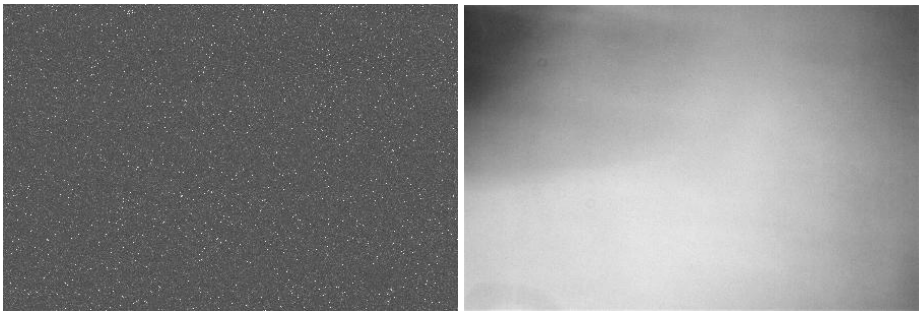

(c) Dark calibration frame (d) Flat calibration frame using the V filter

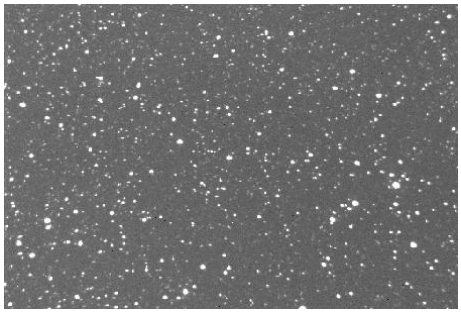

(e) Object frame after processing

Figure 3.1 Before and after images for the starfield of 4U 2206+54, as well as the calibration frames used in that night's processing

frame. The flats must also have a similar header adjustment. Furthermore, these frames must have the header adjusted to contain the subset. The subset is the filter in which the flats have been taken. The command *hedit flat*.fits subset X* is used for this, where *X* is the filter. Then the zero and dark

```
ecl> imhead lph128-001v.fit
lph128-001v.fit[2184,1472][ushort]:
No bad pixels, min=0., max=0. (old)
Line storage mode, physdim [2184,1472], length of user area 1094 s.u.
Created Fri 15:53:35 28-May-2010, Last modified Sun 02:07:16 16-May-2010
Pixel file "lph128-001v.fit" [ok]
BSCALE  =   1.0000000000000000 /physical = BZERO + BSCALE*array_value
BZERO   =   32768.000000000000 /physical = BZERO + BSCALE*array_value
TELESCOP= 'DDT 0.4-m' /         telescope used to acquire this image
INSTRUME= 'SBIG ST-10 Dual CCD Camera'
OBSERVAT= 'esc     '
DATE-OBS= '2010-05-16T08:06:17' /YYYY-MM-DDThh:mm:ss observation start, UT
EXPTIME =   50.000000000000000 /Exposure time in seconds
EXPOSURE=   50.000000000000000 /Exposure time in seconds
SET-TEMP=  -15.000000000000000 /CCD temperature setpoint in C
CCD-TEMP=  -15.233190954856305 /CCD temperature at start of exposure in C
XPIXSZ  =   6.8000000000000007 /Pixel Width in microns (after binning)
YPIXSZ  =   6.8000000000000007 /Pixel Height in microns (after binning)
XBINNING=                    1 /Binning factor in width
YBINNING=                    1 /Binning factor in height
XORGSUBF=                    0 /Subframe X position in binned pixels
YORGSUBF=                    0 /Subframe Y position in binned pixels
FILTER  = 'V       ' /          Filter used when taking image
IMAGETYP= 'Light Frame' /       Type of image
SITELAT = '40 14 50' /          Latitude of the imaging location
SITELONG= '-111 39 02' /        Longitude of the imaging location
EGAIN   =   1.3600000143051147 /Electronic gain in e-/ADU
FOCALLEN=   1624.0000000000000 /Focal length of telescope in mm
APTDIA  =   406.00000000000000 /Aperture diameter of telescope in mm
APTAREA =   128167.27634444808 /Aperture area of telescope in mm^2
SWCREATE= 'MaxIm DL Version 4.51' /Name of software that created the image
SBSTDVER= 'SBFITSEXT Version 1.0' /Version of SBFITSEXT standard in effect
SWOWNER = 'Eric G. Hintz' /     Licensed owner of software
ecl>
```

Figure 3.2 Header before additions

```
daophot> imhead lph1280001.fits
lph1280001.fits[2184,1472][real]: lph128
No bad pixels, min=0., max=0. (old)
Line storage mode, physdim [2184,1472], length of user area 2673 s.u.
Created Thu 16:08:21 27-May-2010, Last modified Thu 16:08:20 27-May-2010
Pixel file "lph1280001.fits" [ok]
EXTEND  =                    F / File may contain extensions
ORIGIN  = 'NOAO-IRAF FITS Image Kernel July 2003' / FITS file originator
OBJECT  = 'lph128  '           / Name of the object observed
DATE    = '2010-05-27T22:08:21' / Date FITS file was generated
IRAF-TLM= '2010-05-27T22:08:20' / Time of last modification
TELESCOP= 'DDT 0.4-m' /         telescope used to acquire this image
INSTRUME= 'SBIG ST-10 Dual CCD Camera'
DATE-OBS= '2010-05-16T08:06:17' /YYYY-MM-DDThh:mm:ss observation start, UT
EXPTIME =   50.000000000000000 /Exposure time in seconds
EXPOSURE=   50.000000000000000 /Exposure time in seconds
SET-TEMP=  -15.000000000000000 /CCD temperature setpoint in C
CCD-TEMP=  -15.233190954856305 /CCD temperature at start of exposure in C
XPIXSZ  =   6.8000000000000007 /Pixel Width in microns (after binning)
YPIXSZ  =   6.8000000000000007 /Pixel Height in microns (after binning)
XBINNING=                    1 /Binning factor in width
YBINNING=                    1 /Binning factor in height
XORGSUBF=                    0 /Subframe X position in binned pixels
YORGSUBF=                    0 /Subframe Y position in binned pixels
FILTER  = 'V       ' /          Filter used when taking image
SITELAT = '40 14 50' /          Latitude of the imaging location
SITELONG= '-111 39 02' /        Longitude of the imaging location
EGAIN   =   1.3600000143051147 /Electronic gain in e-/ADU
FOCALLEN=   1624.0000000000000 /Focal length of telescope in mm
APTDIA  =   406.00000000000000 /Aperture diameter of telescope in mm
APTAREA =   128167.27634444808 /Aperture area of telescope in mm^2
SWCREATE= 'MaxIm DL Version 4.51' /Name of software that created the image
SBSTDVER= 'SBFITSEXT Version 1.0' /Version of SBFITSEXT standard in effect
SWOWNER = 'Eric G. Hintz' /     Licensed owner of software
SUBSET  = 'V       '
RA      = '22:07:57.05'
DEC     = '54:31:05.80'
EPOCH   = '2000    '
IMAGETYP= 'object  '
OBSERVER= 'E.Hintz '
OBS     = '@observat'
OBSERVAT= 'esc     '
ST      = '16:15:25.63'
JD      =    2455332.83798611
HJD     =     2455332.8359274
LJD     =           2455332.
AIRMASS =            1.845629
UTMIDDLE= '2010-05-16T08:06:42.00'
WCSDIM  =                    2
LTM1_1  =                   1.
LTM2_2  =                   1.
WAT0_001= 'system=physical'
WAT1_001= 'wtype=linear'
WAT2_001= 'wtype=linear'
ZEROCOR = 'May 27 16:08 Zero level correction image is Zero.fits'
DARKCOR = 'May 27 16:08 Dark count correction image is Dark.fits with scale=0.7'
FLATCOR = 'May 27 16:08 Flat field image is FlatV.fits with scale=27191.52'
CCDSEC  = '[1:2184,1:1472]'
CCDPROC = 'May 27 16:08 CCD processing done'
daophot>
```

Figure 3.3 Header after additions

master frames are applied to the flats. Finally the flats can be combined to form the master flat frame. These master frames are then applied to the object frames using the command *ccdproc*. The ccdproc task has several parameters that must be changed before the master frames can be applied. A typical list of parameters is shown in Figure 3.5.

Once the object frames have been processed, an object image is then displayed in ds9. On the image, a distribution of comparison stars is selected. This distribution should include the target star(s) as well as stable stars. See Table 3.1 for a list of all the stars used in our photometry. IRAF can then measure the counts of the sky in a chosen annulus, which are then subtracted from

```
daophot> imhead zero0001.fits
zero0001.fits: Cannot open image (zero0001.fits)
daophot> pwd
/home/jbugno
daophot> imhead zero0001.fits
zero0001.fits[2184,1472][ushort]:
No bad pixels, min=43., max=5663.
Line storage mode, physdim [2184,1472], length of user area 2673 s.u.
Created Thu 16:00:08 27-May-2010, Last modified Thu 16:02:30 27-May-2010
Pixel file "zero0001.fits" [ok]
EXTEND  =                    F / File may contain extensions
BSCALE  =          1.000000E0 / REAL = TAPE*BSCALE + BZERO
BZERO   =          3.276800E4 /
ORIGIN  = 'NOAO-IRAF FITS Image Kernel July 2003' / FITS file originator
DATE    = '2010-05-27T22:00:08' / Date FITS file was generated
IRAF-TLM= '2010-05-27T22:02:30' / Time of last modification
DATAMIN =                 43. / Minimum data value
DATAMAX =               5663. / Maximum data value
TELESCOP= 'DDT 0.4-m' /         telescope used to acquire this image
INSTRUME= 'SBIG ST-10 Dual CCD Camera'
OBSERVAT= 'esc     '
DATE-OBS= '2010-05-16T03:15:45' /YYYY-MM-DDThh:mm:ss observation start, UT
EXPTIME =  0.00000000000000000 /Exposure time in seconds
EXPOSURE=  0.00000000000000000 /Exposure time in seconds
SET-TEMP=  -15.000000000000000 /CCD temperature setpoint in C
CCD-TEMP=  -14.809516780639790 /CCD temperature at start of exposure in C
XPIXSZ  =   6.8000000000000007 /Pixel Width in microns (after binning)
YPIXSZ  =   6.8000000000000007 /Pixel Height in microns (after binning)
XBINNING=                    1 /Binning factor in width
YBINNING=                    1 /Binning factor in height
XORGSUBF=                    0 /Subframe X position in binned pixels
YORGSUBF=                    0 /Subframe Y position in binned pixels
IMAGETYP= 'zero    '           /        Type of image
SITELAT = '40 14 50' /          Latitude of the imaging location
SITELONG= '-111 39 02' /        Longitude of the imaging location
EGAIN   =   1.3600000143051147 /Electronic gain in e-/ADU
FOCALLEN=   1624.0000000000000 /Focal length of telescope in mm
APTDIA  =   406.00000000000000 /Aperture diameter of telescope in mm
APTAREA =   128167.27634444808 /Aperture area of telescope in mm^2
SWCREATE= 'MaxIm DL Version 4.51' /Name of software that created the image
SBSTDVER= 'SBFITSEXT Version 1.0' /Version of SBFITSEXT standard in effect
SWOWNER = 'Eric G. Hintz' /     Licensed owner of software
daophot>
```

Figure 3.4 This is a typical header for a zero calibration frame.

the counts from the star in a chosen aperture. This value is then divided by the exposure time, and then a chosen zero point is added in to compute instrumental magnitudes for each star using the command *phot*. Apertures and annuli were determined by reviewing the radial profile of the stars. If any unstable stars are chosen, they can be taken out using a program called *varstar* (Hintz 2010). *Varstar* is also used to create differential magnitudes. The differential magnitude of a star is calculated by first taking the average instrumental magnitude from all stable stars in the distribution. This value is then subtracted from the instrumental magnitude of every star for every observation, creating the differential magnitude. For the specific starfield for 4U 2206+54, not

```
                                                                                Image Reduction and Analysis Facility
PACKAGE = ccdred
   TASK = ccdproc

images  = ▉       lph128*.fits  List of CCD images to correct
(output =                     ) List of output CCD images
(ccdtype=               object) CCD image type to correct
(max_cac=                    0) Maximum image caching memory (in Mbytes)
(noproc =                   no) List processing steps only?

(fixpix =                   no) Fix bad CCD lines and columns?
(oversca=                   no) Apply overscan strip correction?
(trim   =                   no) Trim the image?
(zerocor=                  yes) Apply zero level correction?
(darkcor=                  yes) Apply dark count correction?
(flatcor=                  yes) Apply flat field correction?
(illumco=                   no) Apply illumination correction?
(fringec=                   no) Apply fringe correction?
(readcor=                   no) Convert zero level image to readout correction?
(scancor=                   no) Convert flat field image to scan correction?

(readaxi=                 line) Read out axis (column|line)
(fixfile=                     ) File describing the bad lines and columns
(biassec=                     ) Overscan strip image section
(trimsec=                     ) Trim data section
(zero   =            Zero.fits) Zero level calibration image
(dark   =            Dark.fits) Dark count calibration image
(flat   =                Flat*) Flat field images
(illum  =                     ) Illumination correction images
(fringe =                     ) Fringe correction images
(minrepl=                   1.) Minimum flat field value
(scantyp=           shortscan) Scan type (shortscan|longscan)
(nscan  =                   1) Number of short scan lines

(interac=                   no) Fit overscan interactively?
(functio=            legendre) Fitting function
(order  =                   1) Number of polynomial terms or spline pieces
(sample =                   *) Sample points to fit
(naverag=                   1) Number of sample points to combine
(niterat=                   1) Number of rejection iterations
(low_rej=                   3.) Low sigma rejection factor
(high_re=                   3.) High sigma rejection factor
(grow   =                   0.) Rejection growing radius
(mode   =                   ql)
```

Figure 3.5 This is a list of parameters used for the task *ccdproc* on object frames.

only must the target star be taken out, but the δ Scuti variable and an eclipsing binary must also be removed. Furthermore, it is possible that a stable star may move onto a bad pixel. In this case, this star must be removed as well.

Table 3.1. Celestial Coordinates of Chosen Stars

Star Name	RA (h:m:s)	Dec (d:m:s)	V	B - V	V - R	V - I
†‡4U 2206+54	22:07:57.24	+54:31:06.40	9.902	0.262	0.214	0.431
‡BD +53 2792	22:08:20.75	+54:30:33.20	10.452	0.253	0.146	0.290
‡GSC 03973-01066	22:08:25.40	+54:29:06.70	11.922	0.233	0.139	0.296
‡GSC 03973-01906	22:08:44.91	+54:28:01.42	11.825	0.540	0.330	0.653
N1AZ043319	22:08:15.45	+54:28:56.19				
N1AZ000743	22:07:48.24	+54:30:16.95				
‡N1AZ000617	22:07:49.18	+54:34:58.3	13.288	0.929	0.526	1.065
‡N1AZ000622	22:07:37.56	+54:34:49.1	12.378	0.911	0.535	0.979
†‡GSC 03973-01698	22:08:41.22	+54:33:09.16	11.114	0.448	0.257	0.523
‡N1AZ000664	22:08:31.88	+54:32:55.80	12.694	0.694	0.392	0.785
‡N1AZ000575	22:08:31.90	+54:36:20.2	11.353	0.536	0.314	0.629
‡N1AZ000589	22:08:23.98	+54:35:55.3	12.803	0.587	0.353	0.708
N1AZ000745	22:08:25.24	+54:30:09.9				
N1AZ000644	22:07:59.07	+54:33:53.5				
N1AZ056050	22:07:32.74	+54:35:54.5				
GSC 03973-01692	22:07:26.11	+54:30:42.0				
‡N1AZ000794	22:08:44.91	+54:28:01.4	11.867	0.464	0.259	0.510
N1AZ000580	22:08:47.35	+54:36:13.3				
N1AZ000573	22:09:04.67	+54:36:31.1				
N1AZ000593	22:09:09.81	+54:35:45.7				
N1AZ000556	22:09:17.23	+54:37:37.9				
N1AZ000724	22:08:58.05	+54:30:43.2				
N1AZ000812	22:09:02.83	+54:27:05.8				
N1AZ054968	22:08:37.36	+54:35:12.5				
N1AZ000798	22:08:05.05	+54:27:52.1				
N1AZ041069	22:08:49.51	+54:27:39.2				
N1AZ000750	22:07:18.21	+54:30:01.6				
‡N1AZ047429	22:07:12.26	+54:31:12.9	12.640	0.298	0.183	0.395
N1AZ000749	22:06:55.65	+54:30:02.5				
N1AZ000669	22:06:53.47	+54:32:48.2				
N1AZ000659	22:06:55.47	+54:33:15.9				

Table 3.1 (continued)

Star Name	RA (h:m:s)	Dec (d:m:s)	V	B - V	V - R	V - I
‡N1AZ000636	22:07:02.79	+54:35:10.5	10.131	0.984	0.572	1.080
‡N1AZ000557	22:07:03.59	+54:37:24.4	11.363	0.645	-2.355	0.796
‡N1AZ058792	22:08:11.80	+54:37.24.9	13.169	0.587	0.356	0.721
‡N1AZ000816	22:08:13.07	+54:26:55.1	13.619	1.052	0.694	1.353
N1AZ000016	22:07:36.84	+54:21.53.5				
N1AZ000862	22:07:05.06	+54:23:47.9				
N1AZ000840	22:06:50.52	+54:25:11.0				
N1AZ000644	22:07:59.10	+54:33:53.6				
N1AZ000819	22:06:50.28	+54:26:50.4				
N1AZ000723	22:07:14.27	+54:30:49.2				
N1AZ000661	22:08:58.50	+54:33:08.6				
N1AZ055509	22:08:42.92	+54:35:21.5				
N1AZ049151	22:06:35.37	+54:31:06.4				
N1AZ000681	22:06:34.36	+54:32:24.8				
N1AZ050229	22:07:38.95	+54:32:51.5				
N1AZ034055	22:08:02.71	+54:23:45.0				
N1AZ000808	22:07:40.43	+54:27:29.1				
N1AZ052427	22:08:36.60	+54:33:40.3				
N1AZ000834	22:08:49:04	+54:25:24.6				
N1AZ036871	22:07:52.67	+54:25:31.4				
N1AZ036811	22:07:22.57	+54:25:34.3				
N1AZ050810	22:08:20.24	+54:32:52.8				
N1AZ000687	22:09:02:41	+54:32:05.3				
‡N1AZ039290	22:07:42.66	+54:26:56.2	14.789	1.889	1.270	2.416
‡N1AZ037363	22:07:27.97	+54:25:54.0	14.143	0.767	0.424	0.849
‡N1AZ041758	22:07:02.98	+54:28:29.3	14.607	1.747	1.187	2.201
‡N1AZ057448	22:07:51.68	+54:36:41.9	14.559	0.494	0.301	0.654
N1AZ051172	22:07:10.88	+54:33:33.8				
N1AZ052577	22:07:19.42	+54:34:08.5				

Note. — †designates 4U 2206+54 and GSC 03973-01698. ‡designates standardized field stars from September 26, 2010.

3.2 Standardization

In order to see true variation in the variable targets, reliable magnitudes in B, V, R, and I needed to be calculated. To do this, we first observed a standard star field at several different airmasses throughout one night. The airmass should vary between 1 airmass (at the zenith) and 2 airmasses (approximately 30° above the horizon). This type of standard field is known as an extinction field. It was necessary to have a photometric night (absolutely no clouds) for this process, otherwise the calculated magnitudes may be incorrect due to cirrus clouds that our eyes cannot perceive. The target star fields are then sandwiched between the standard field observations. We used the WMO 0.9 m telescope on September 26, 2010 for the standards star observation. As is described later, secondary standard stars were created for other nights.

As mentioned in Section 3.1, the *phot* command will calculate instrumental magnitudes of the selected stars. This, as well as the typical reduction methods, must be done for the well known stars in the extinction field. The field used for this project was the Landolt standard field SA114 (Landolt 1992). Once processed and "photted," a plot can be made for each star containing instrumental magnitude vs. airmass. This should be linear, as seen in Figure 3.6. The slope of this line reveals how many magnitudes per airmass have been lost. Now the following equation can be used to correct for observations taken at different airmasses:

$$m_2 = m_1 - airmass * slope \tag{3.1}$$

where m_1 is the instrumental magnitude calculated in IRAF. Equation 3.1 must be applied to each instrumental magnitude of each star for each filter used. While the values can be averaged together within the same filter, the values cannot be averaged from filter to filter.

Using the catalog magnitudes of the standard stars, a zero point was calculated. To find the zero point, the values for m_2 are averaged, $\langle m_2 \rangle$, for each of the selected stars. Equation 3.2 was

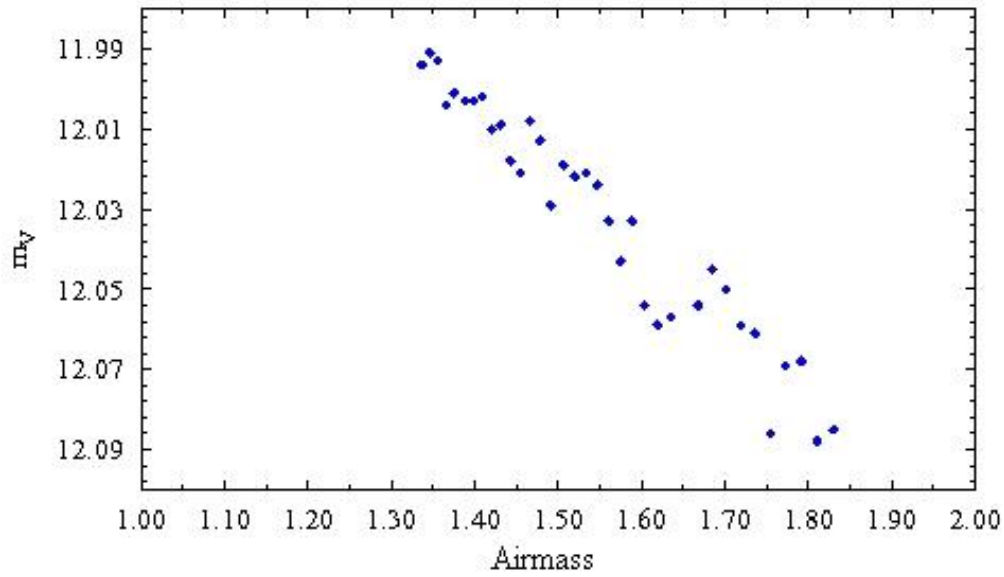

Figure 3.6 This is a typical instrumental magnitude vs. airmass graph. This particular graph is for Star 4 in our distribution.

then used to determine the zero point (ZP) for the V filter:

$$ZP = \langle m_2 \rangle - V \tag{3.2}$$

where V is the published magnitude for the chosen Landolt standard stars. Equation 3.2 must be used for each standard star. Once the ZP values have been calculated, a ZP vs. color plot can be created. The normal color values are either $B-V$, $V-R$, or $R-I$. If the trend is scattered, but mostly flat, then the average ZP is determined and applied in the following equation to all the instrumental magnitudes:

$$m = m_i - (airmass * extinction) + (B-V)A + ZP \tag{3.3}$$

where A is the slope of the color-zero point plot, and the extinction is the slope of the airmass plot. If the trend is a horizontal line, the $(B-V)A$ term vanishes because $A = 0$. However, if the trend

is not a horizontal line, this term remains, and is referred to as a color term. There was a small slope in the zero point graph for the OPO data and WMO data, as seen in Figure 3.7, so a color term was considered in the each magnitude correction equation for the different observatories. The

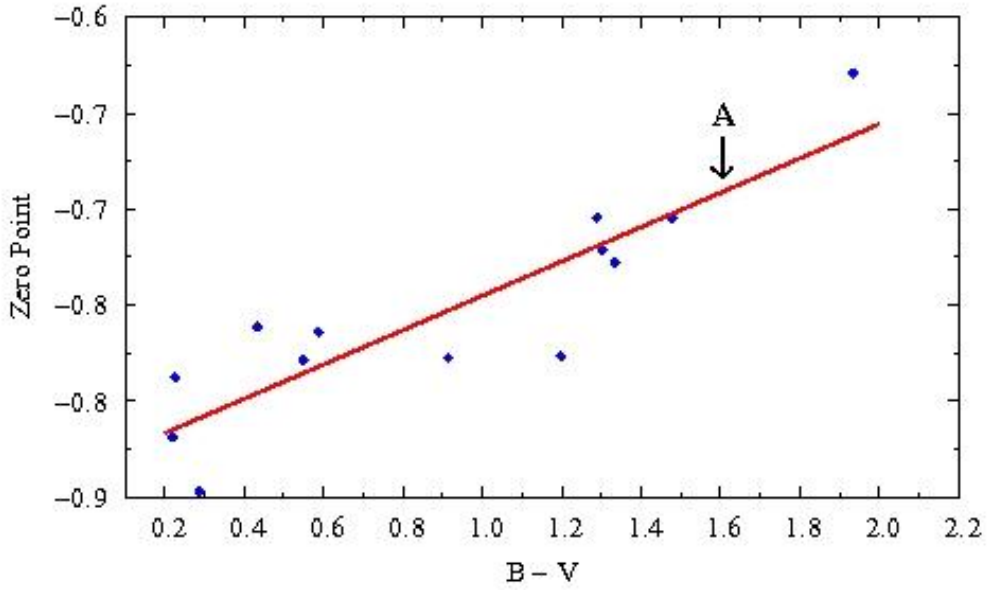

Figure 3.7 This graph shows the zero point vs. color trend for data taken at WMO. The red line is the best fit line, used in Equation 3.3.

color term will not always be $B-V$, but rather will change depending on the filter for which the magnitudes are being corrected. The color that was used in the zero point plot must also be used in Equation 3.3. This standardization process was done for all B, V, R, and I filters.

Equation 3.3 can also be used to adjust the instrumental magnitude for the selected distribution stars. For this project, 20 stars were chosen for the distribution. Since multiple telescopes were used to gather data for this project, different CCD's were used. These CCD's do not have the same field of view, so some distribution stars differ since it was necessary to keep 20 in the group to maintain a decent sample size. This was noted for each group, and taken care of during

standardization.

After *varstar* has been run on the data, IRAF will create a name.log file. In this file, one can find a column called mag2, as seen in Figure 3.8. Mag2 values are the average differential magnitude

```
Processing of file : lph128.lst
Starting HJD = 2455368.7436
Ending HJD = 2455368.8298
Filter : I

  ID   mag1   error1   mag2   error2
   1 -2.3121  0.0052  0.3836  0.0050  *
   2 -1.5946  0.0105  1.1011  0.0107  *
   3 -0.1038  0.0102  2.5919  0.0095
   4 -0.5470  0.0073  2.1487  0.0067
   5  1.6965  0.0352  4.3922  0.0349  *
   6 -0.8474  0.0057  1.8483  0.0055
   7 -1.1665  0.0136  1.5292  0.0138  *
   8  0.1696  0.0100  2.8653  0.0100
   9 -0.3994  0.0109  2.2963  0.0109  *
  10 -0.0326  0.0111  2.6631  0.0113
  11 -0.2407  0.0124  2.4550  0.0123  *
  12 -0.5846  0.0119  2.1111  0.0117  *
  13 -0.1952  0.0080  2.5005  0.0077
  14 -0.3109  0.0088  2.3848  0.0085
  15  0.9374  0.0207  3.6331  0.0205  *
  16  0.6369  0.0138  3.3326  0.0143
  17  0.4394  0.0139  3.1351  0.0141
  18  0.5582  0.0169  3.2539  0.0165  *
  19  0.2674  0.0123  2.9631  0.0126
  20  0.5236  0.0134  3.2193  0.0140

Ensemble Average 12.7421 +-  0.0443
Super Star Avg. = 10.0464 +-  0.0444
Airmass Information :
Rcorr =  0.1410
Beta1 =  0.0406 +-  0.0463
Beta0 = 12.6808 +-  0.0702
```

Figure 3.8 This is the .log file for June 21, 2010 in the I filter. The stars denoted with an $*$ have been removed from the distribution.

for each star. Mag2 values are determined based on fluxes. This is important because dimmer stars will contribute less.

At this point, adjusting the differential magnitudes was necessary to take into account varying

weather conditions as well as having different stars kept in the distribution. Usually, the same distribution stars are removed, but occasionally stars will move onto bad pixels or drift off the frame. Our adjustment was made using September 26, 2010 as the reference night. This night was chosen as the reference night because it was the night of standard star observations. Therefore, we know the conditions on this night were favorable. Because each of the adjusted nights has its own set of mag2 values, a different correction was made for each. First it was necessary to take an average of the mag2 values of the stable stars left in the distribution. Then the average of the mag2 values for September 26 was calculated, using the same stable stars. The difference in the two averages was then computed. This difference was added to the individual differential magnitudes for the night in question. If accurate, the correction factor added to any stable star should produce an average differential magnitude reasonably close to that of September 26 for that star. Indeed, this was the case for our data. Differences were between a few thousandths to a few hundredths at most.

The next step in the standardization process is calculating the zero point so as to determine apparent magnitudes. Once reliable, standardized apparent magnitudes have been determined, the corresponding mag2 values on a given night can be subtracted from those magnitudes. Now we have a list of magnitudes specific to one filter on one night. Next, we take the average of these specific magnitudes. Stars that were removed in *varstar* are not to be included in this averaging. This is done for each filter for each night. The averaged value is called the calibration constant, or the zero point for that individual night. The mag2 value for each star is added to the calibration constant to give the calculated magnitude for that star. Then, the calculated magnitude for the star is subtracted from the standardized magnitude. This difference is then plotted with color, as seen in Figure 3.9. Figure 3.9 has a red line drawn which signifies the trend of the data points. The equation of the line is then applied to the data using Equation 3.4 to get the apparent magnitude:

$$m = m_{calc} + (color * s + b) \tag{3.4}$$

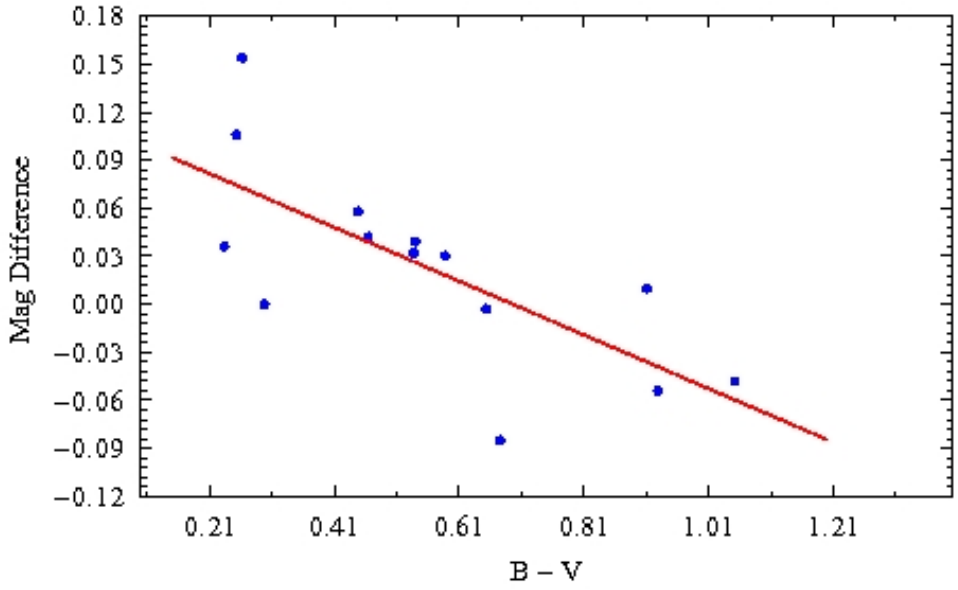

Figure 3.9 This graph represents a typical plot of color and the difference between standardized magnitude and calculated magnitude. This particular plot is for WMO 2010 in the V filter.

Here, s is the slope of the line and b is the y-intercept.

To test our magnitudes, six stars from the starfield of the Seyfert galaxy ZW 229-015 were also photted and processed in the same way. On average, the apparent magnitudes were 0.028 fainter than the published values of Barth et al. (2011). However, all errors were within 3σ. It should be mentioned that Barth et al. (2011) did not consider color in his analysis, but the color is taken into account in our's.

Chapter 4

Results

4.1 Photometric Results

The data collected for 4U 2206+54 were reduced using the process outlined in Chapter 3, and exhibited a definite variation on a long timescale, which is noticeable in the lightcurves. Furthermore, variation was occasionally visible in some individual nights as seen in Figure 4.1. Many of the nights, however, showed only a slight variation which was on the order of several thousandths of a magnitude to one tenth of a magnitude. This small difference is just scatter. Since it was not possible to get many consecutive nights, we saw a period of variability of approximately 25 days from the 2008 data. However, there were four consecutive nights where the magnitude was observed to be changing more rapidly, as in just a few days, than expected as seen in Figure 4.2.

Photometric results from 2009 showed no significant variability of the source during the first few months of the summer. However, it is possible the there was a decrease in magnitude towards the end of the summer, starting at HJD 5063. Other than this possible decrease, no significant variation was observed. Not only did WMO and OPO match for 2009, but the range in magnitude for the δ Scuti, GSC 03973-01698, also remained constant throughout the months of observations.

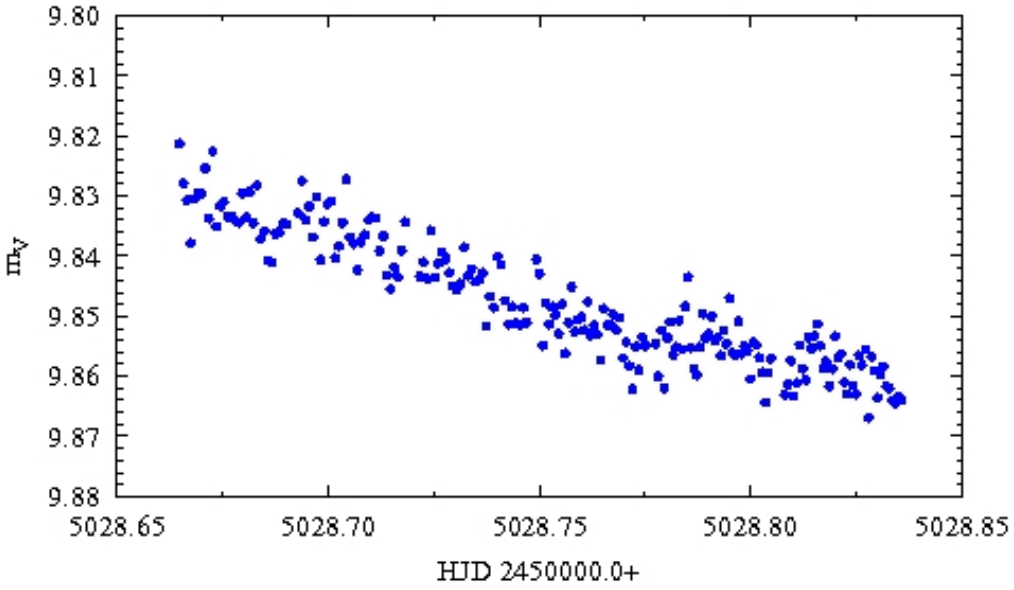

Figure 4.1 This is a lightcurve of 4U 2206+54 from July 16, 2009 using the Orson Pratt Observatory. This night was one of few that showed a noticeable change in brightness.

This leads us to believe that the data analysis for 4U 2206+54 was done correctly. To compare the years of data collection, long term lightcurves for 4U 2206+54 and GSC 03973-01698 can be seen in Figure 4.3 and Figure 4.4 respectively. These graphs are V filter observations only. Furthermore, when V filter data from all three years were placed on the same graph, a slight increase in magnitude was seen across the years, which is evident in Figure 4.5. The red line designates the trend of this increase.

Data from 2010 provided us with a multifilter analysis of 4U 2206+54. A slight variation in the long term lightcurve of the source can be seen in Figure 4.6. It is difficult to tell if the 25.1 day period holds for the 2010 data due to gaps where no observations were taken. The B, V, and I filters all slightly drop in magnitude at HJD 5362 and at HJD 5419, which spans 57 days. It is possible there was another dip that went undetected in the middle of the summer. This would give

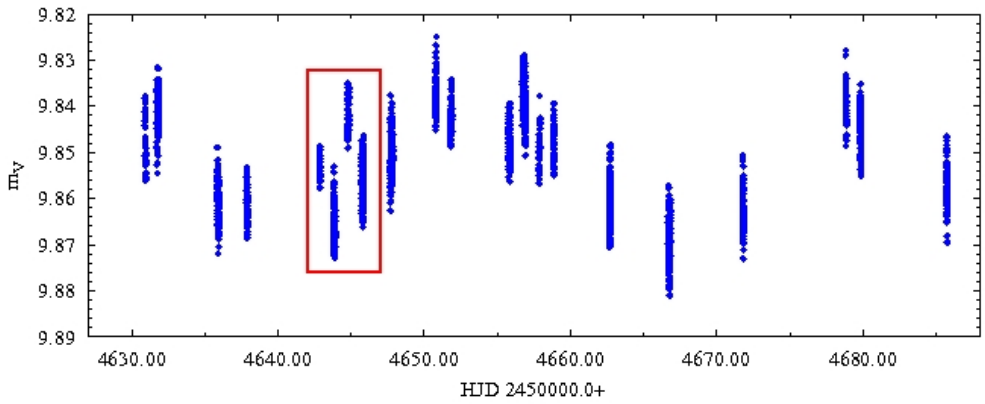

Figure 4.2 This is a long-term graph of 4U 2206+54 for the summer of 2008. Each vertical line is one night of observations taken at the Orson Pratt Observatory. The four consecutive nights mentioned are June 25, 26, 27, and 28, which correspond to HJD's of 4642, 4643, 4644, and 4654 respectively.

a period close to, but not quite, 25.1 d. For comparison, the 2010 multiple filter results for GSC 03973-01698 can be seen in Figure 4.7.

Over the summer of 2010, the *B* filter does not show a significant change, however the first WMO night in the *B* filter, highlighted in Figure 4.8(a), illustrates that sometimes there is variation within a few hours of observation. Figure 4.8(b) displays a stable star in the distribution for comparison. Furthermore, Figure 4.9 includes the 2010 *R* filter observations. The ordinate has been adjusted so that the spread in each filter is the same. The *R* filter had the greatest variation in a single night, which was seen in the first three nights. Upon further investigation into these nights in the *R* filter, it was discovered that those frames were overexposed, which caused the counts per exposure time to become a nonlinear relation. For comparison, Figure 4.10 shows the multifilter WMO plot of GSC 03973-01698. Overexposure explains why the large variation also occurred in the data for GSC 03973-01698.

The two X-ray orbital periods for 4U 2206+54 are 9.6 days (Corbet & Peele 2001) and 19.2 days (Corbet et al. 2007). However, from our 2008 optical data, we see a period of 25.1 days. Phased data from 2008, 2009, and 2010 for all three orbital periods are displayed in Figures 4.11, 4.12, and 4.13 respectively. There is, however, an interesting group of nights during 2008 from an approximate phase of 0.70 to 0.75 that phased well with the 9.6 d period. This group is highlighted in Figure 4.14. This does seem to be a real effect, but this is the only time it is seen. It is possible there is an underlying period of 9.6 d.

Even though the 25.1 d period does not fit 2009 data as neatly as 2008, it still appears to be the best fit of all three periods. In addition, the data from 2009 do not show the small phased feature using the 9.6 d period. For 2010, it is difficult to determine which period fits best due to so few data points.

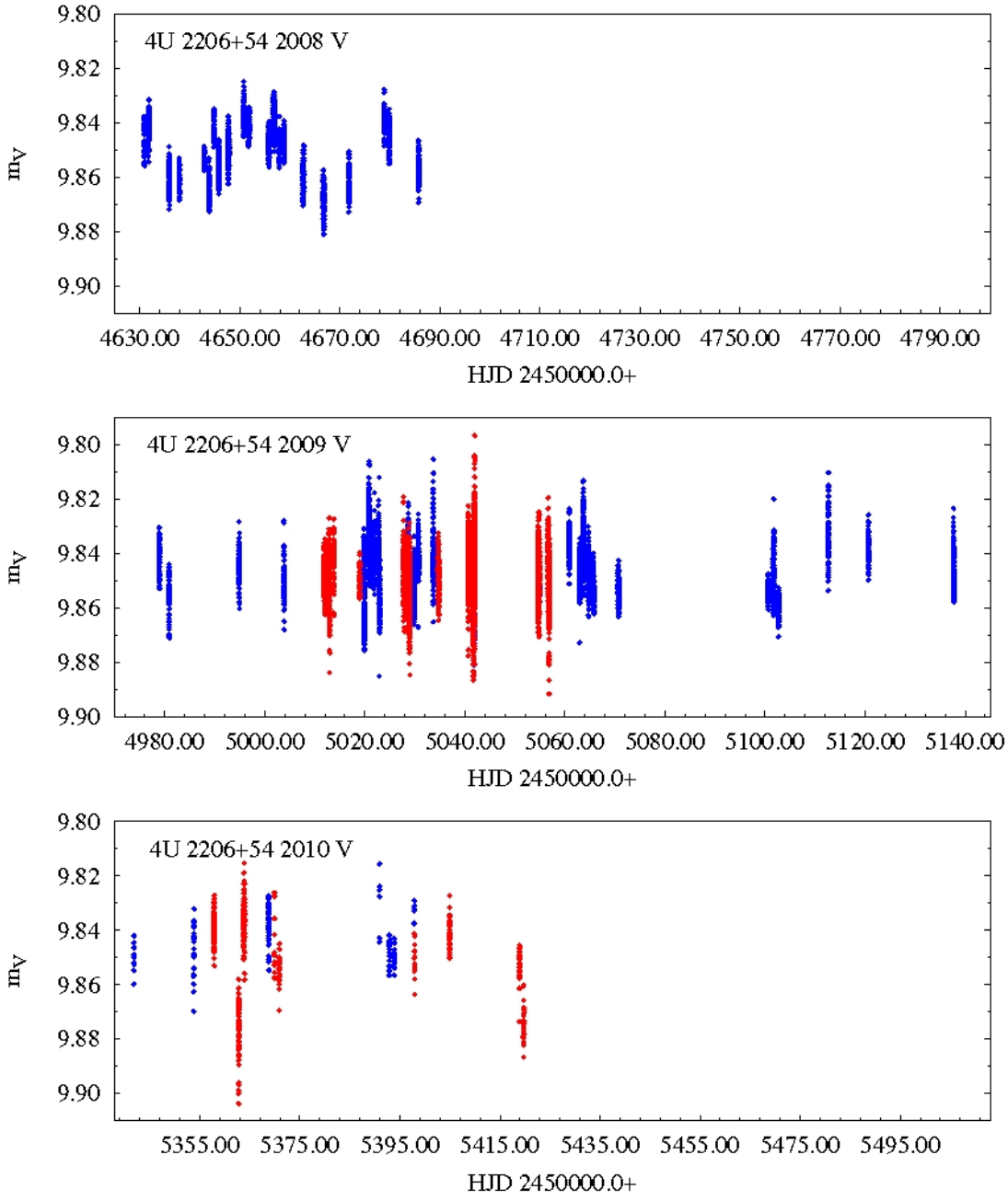

Figure 4.3 This plot displays photometric data from 2008-2010 for 4U 2206+54. All observations were take using the *V* filter. 2008 showed the most significant variation, and both 2009 and 2010 showed slight variation. The ordinate has been adjusted to display the same amount of spread in magnitude in all years. OPO observations are blue, and WMO observations are red.

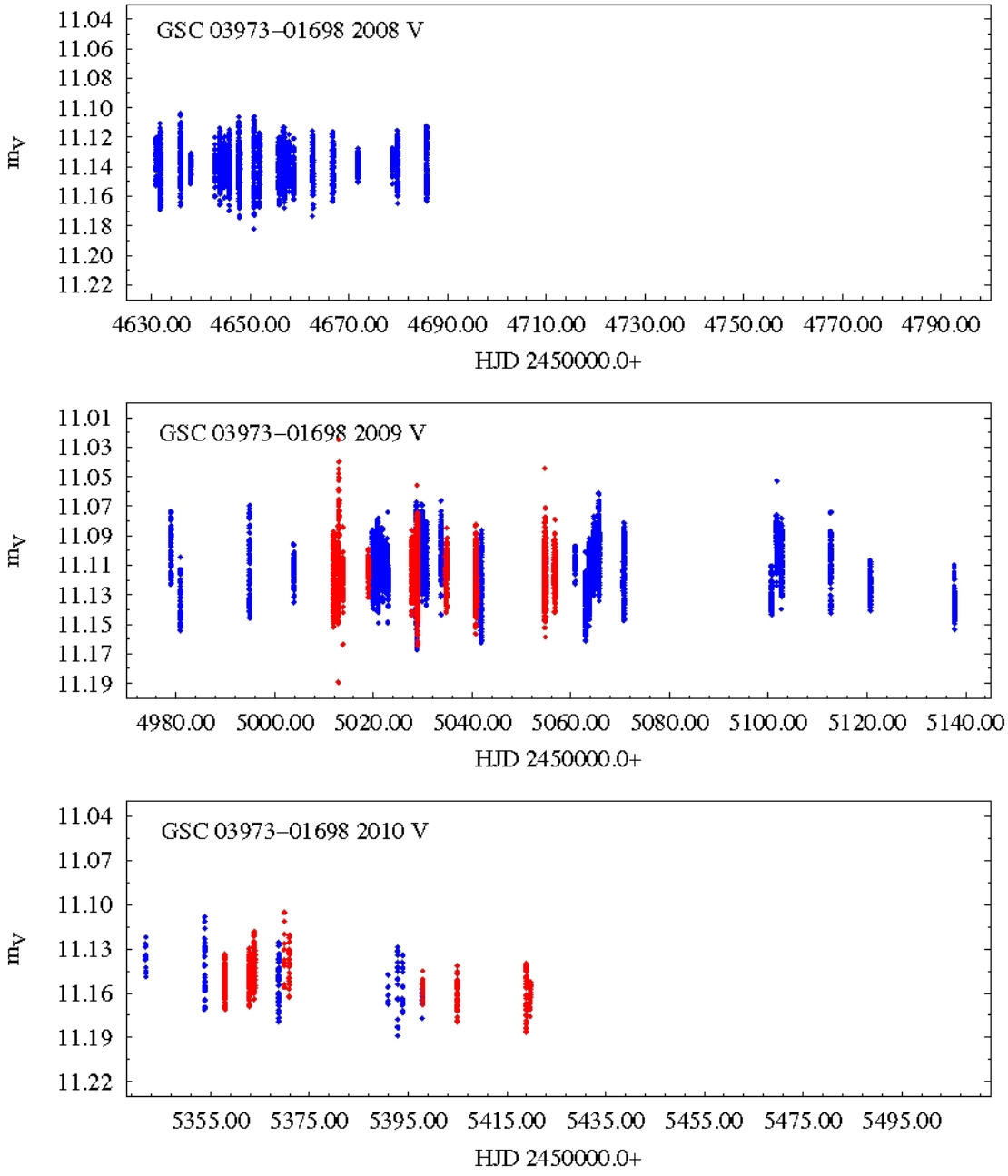

Figure 4.4 This plot displays photometric data from 2008-2010 for GSC 03973-01698. All observations were take using the *V* filter. OPO observations are blue, and WMO observations are red.

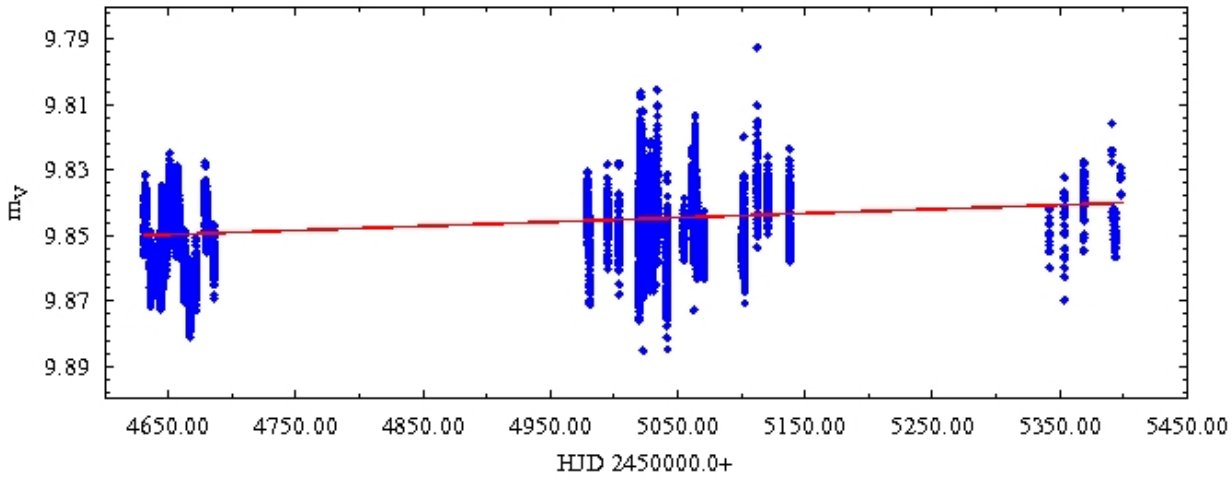

Figure 4.5 This plot shows all the V filter observations for the three years of data.

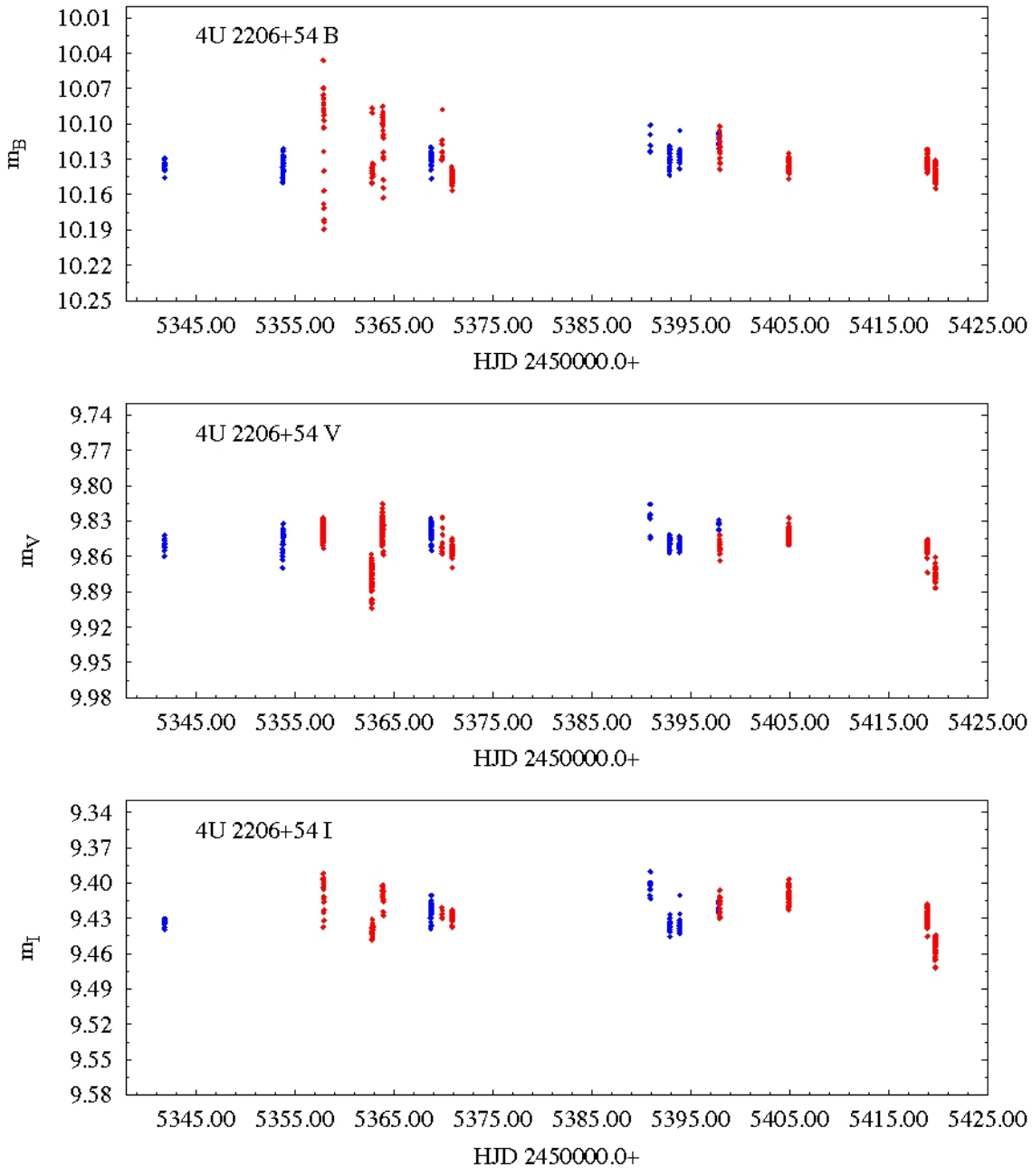

Figure 4.6 This collage displays photometric data from 2010 in the *B*, *V*, and *I* filters of the source 4U 2206+54. The ordinate has been adjusted such that each filter plot has the same amount of spread. OPO observations are blue, and WMO observations are red.

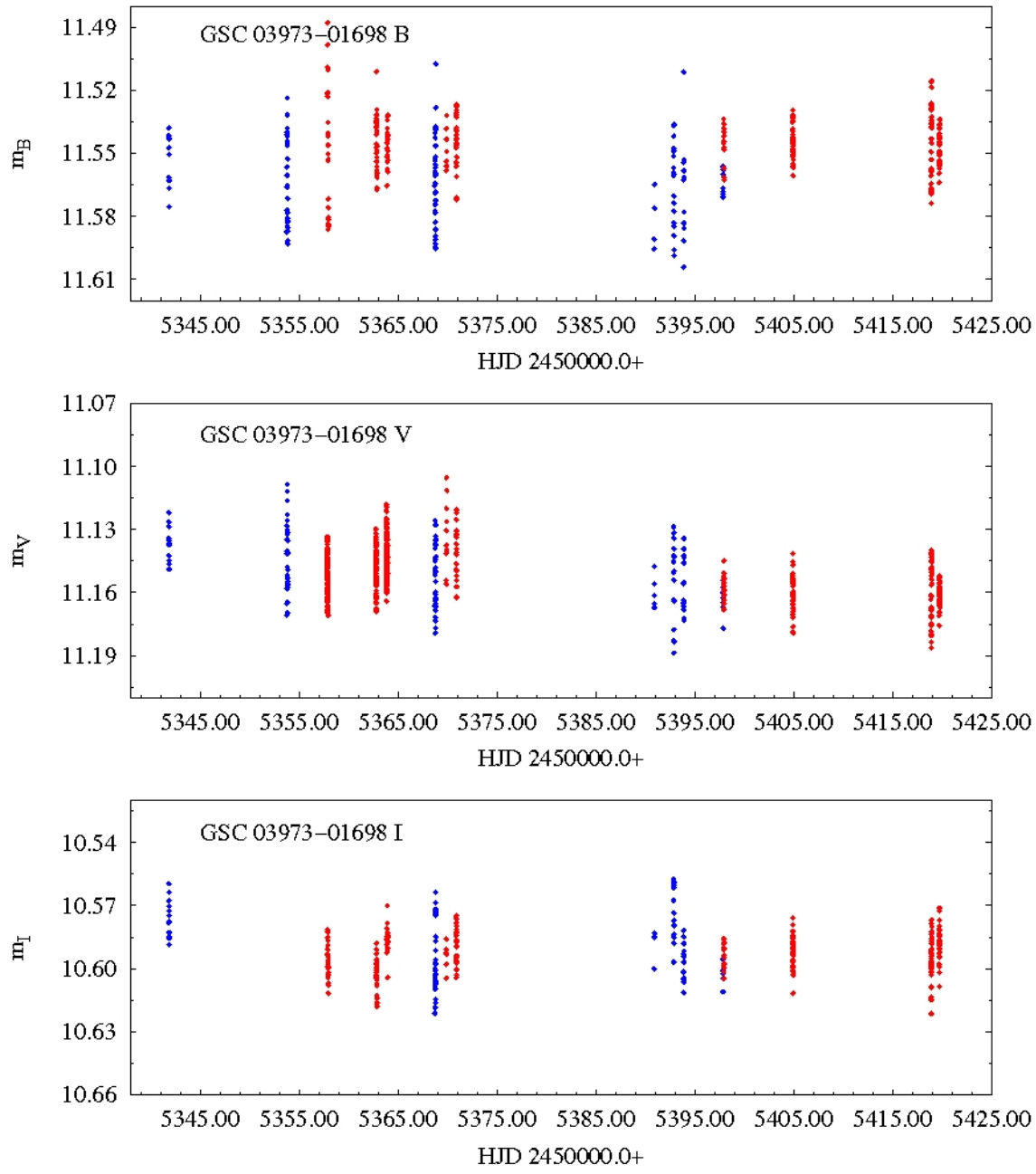

Figure 4.7 This collection of graphs displays photometric data from 2010 in the *B*, *V*, and *I* filters of the delta Scuti GSC 03973-01698. This star is variable on an hourly basis, so the magnitude range appears constant when plotted over several months. OPO observations are blue, and WMO observations are red.

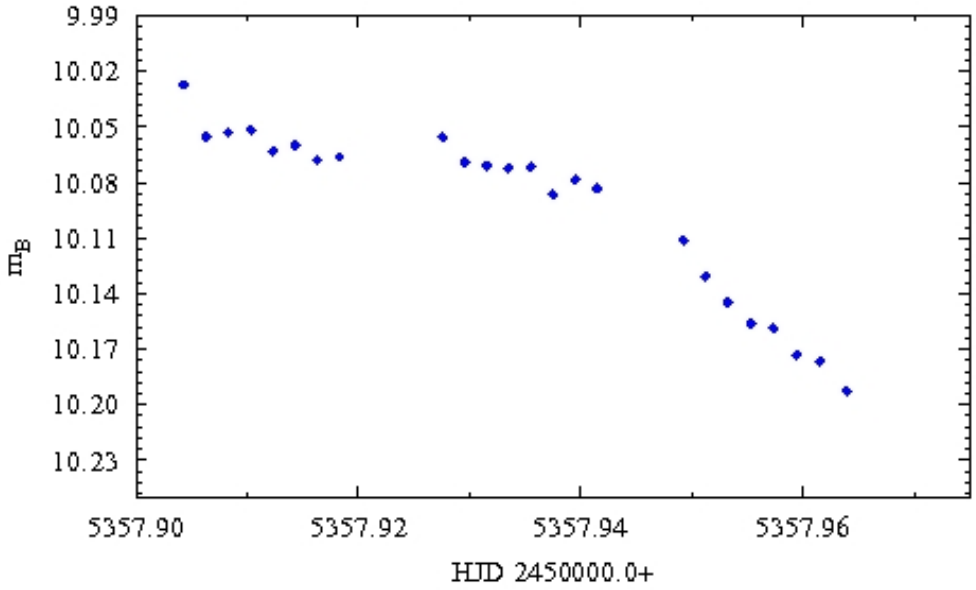

(a) 4U 2206+54 on June 10, 2010

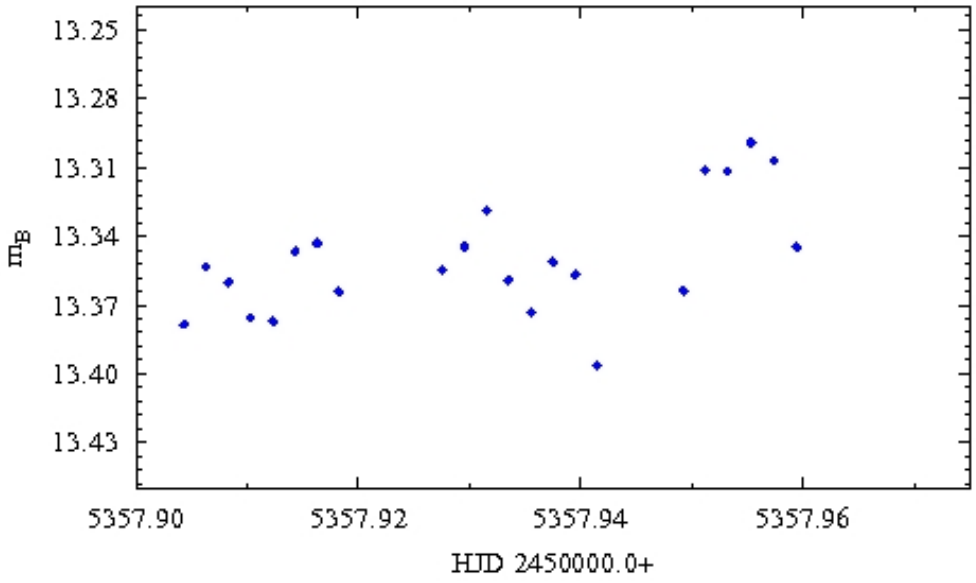

(b) Comparison star on June 10, 2010

Figure 4.8 WMO lightcurves of 4U 2206+54 and Star 8 from the usual distribution stars, taken on June 10, 2010 in the *B* filter

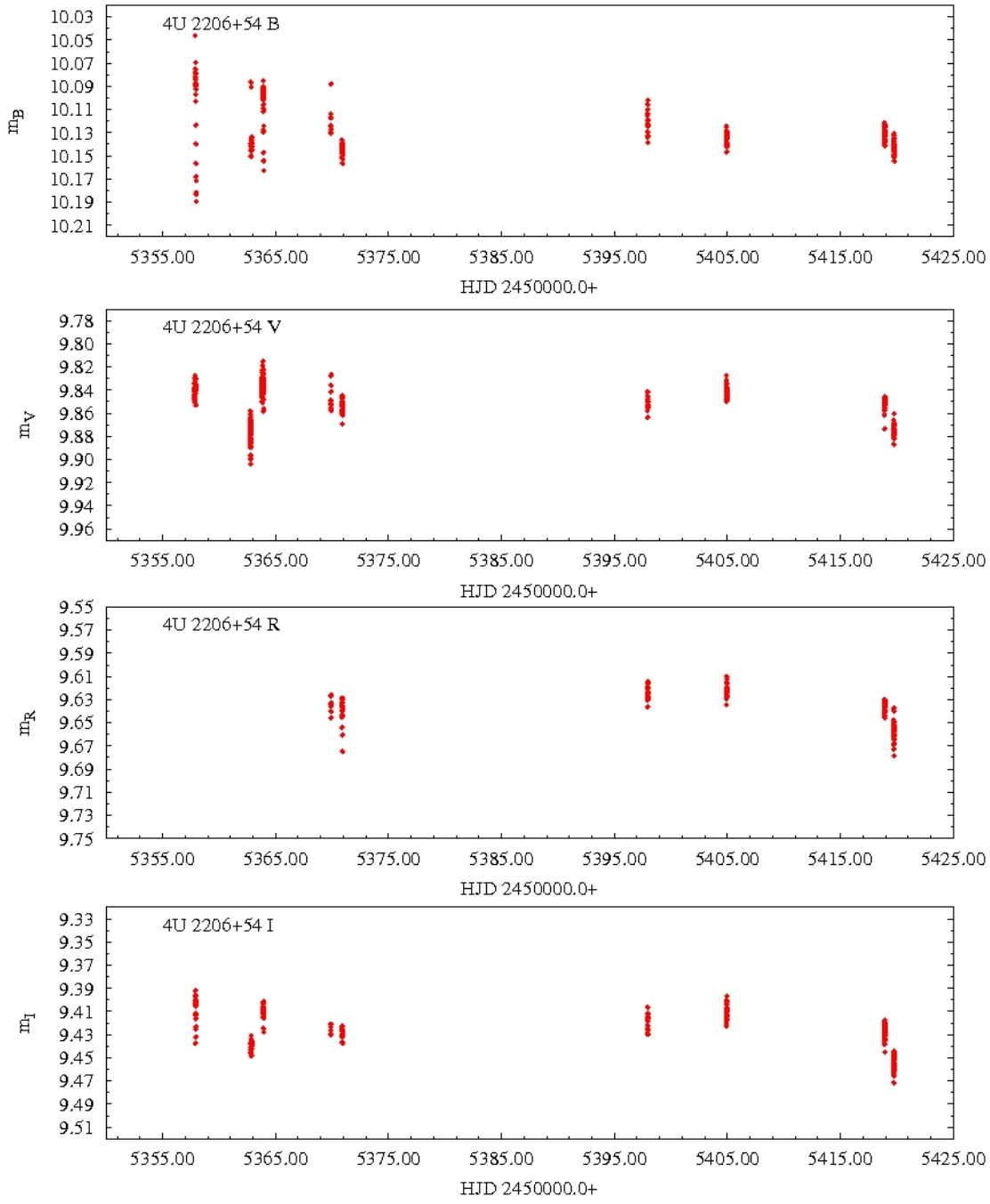

Figure 4.9 These graphs are WMO photometric data from 2010 in the *B*, *V*, *R*, and *I* filters for 4U 2206+54. The three overexposed nights in the *R* filter have been removed.

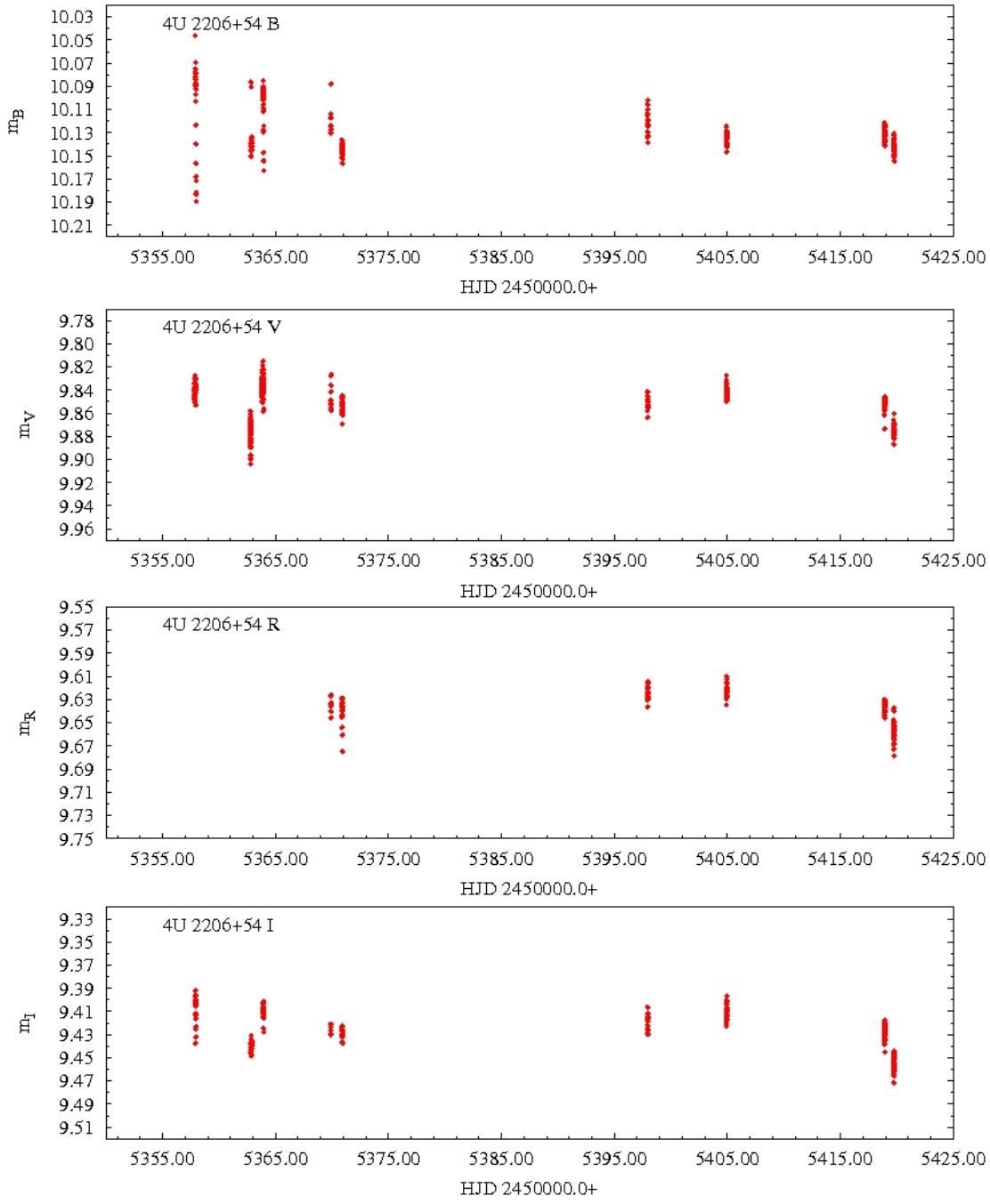

Figure 4.10 These graphs are WMO photometric data from 2010 in the *B*, *V*, *R*, and *I* filters for GSC 03973-01698. The three overexposed nights in the *R* filter have been removed.

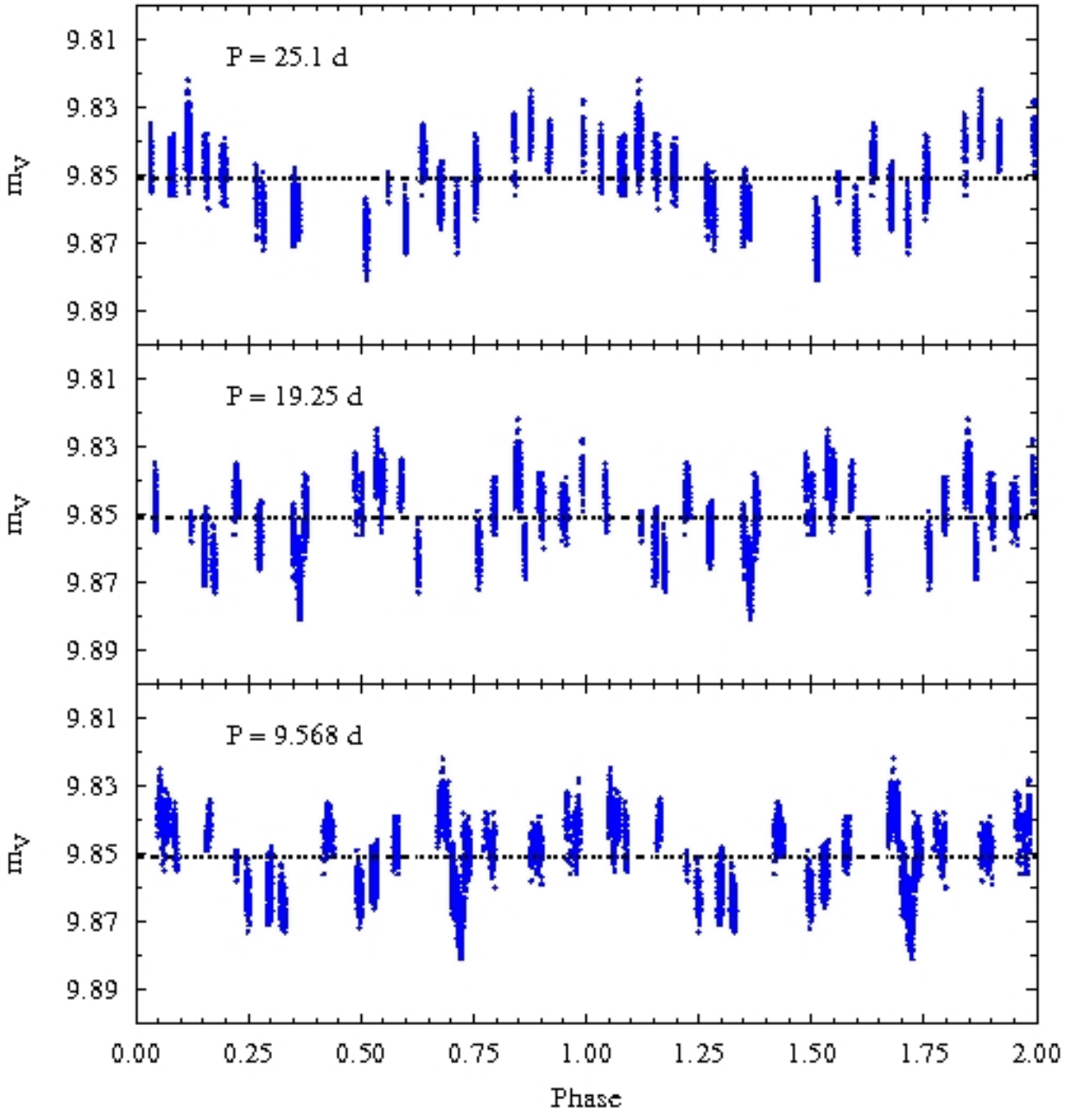

Figure 4.11 2008 data phased with the 9.6 d, 19.2 d, and 25.1 d periods

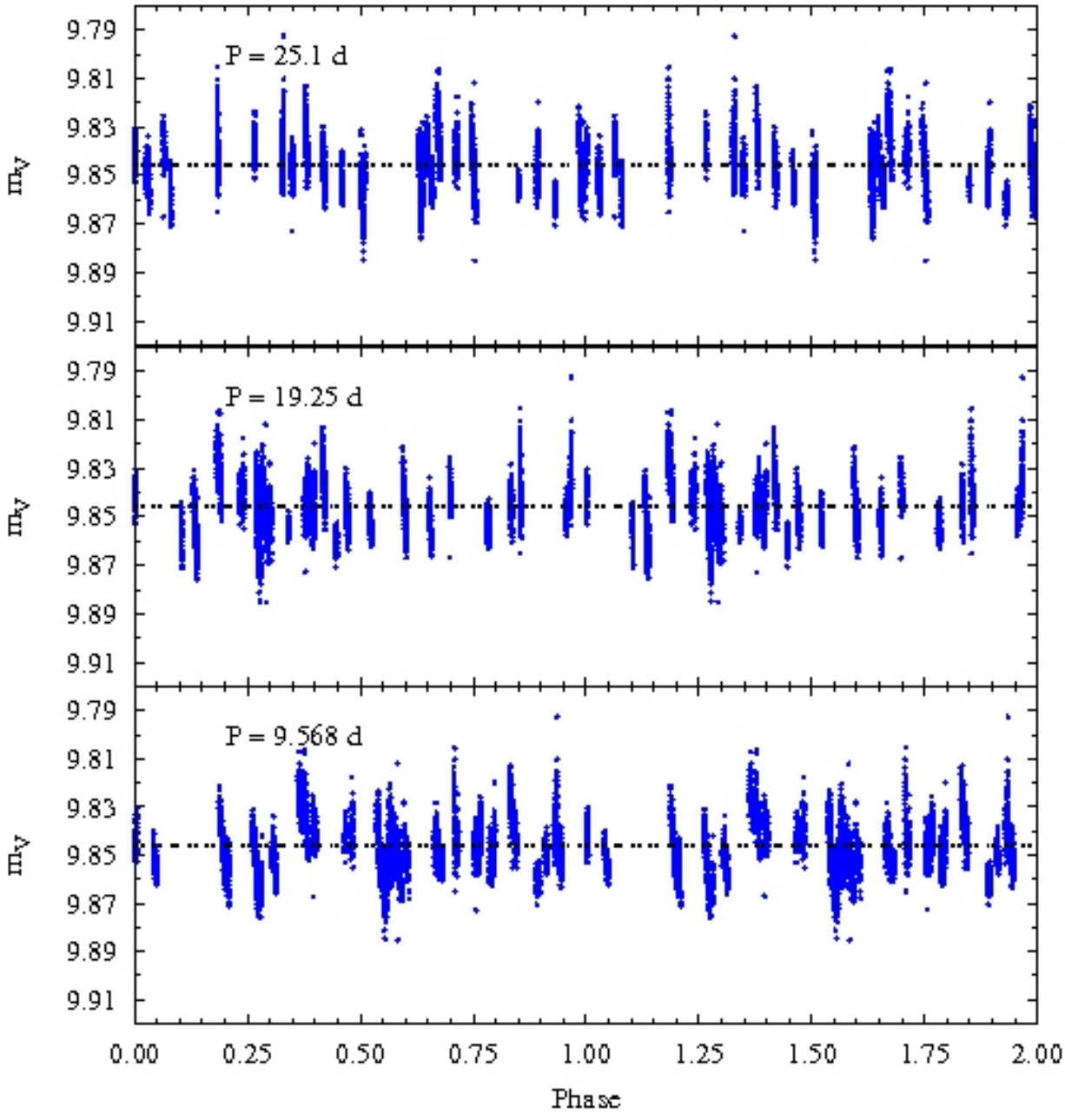

Figure 4.12 2009 data phased with the 9.6 d, 19.2 d, and 25.1 d periods

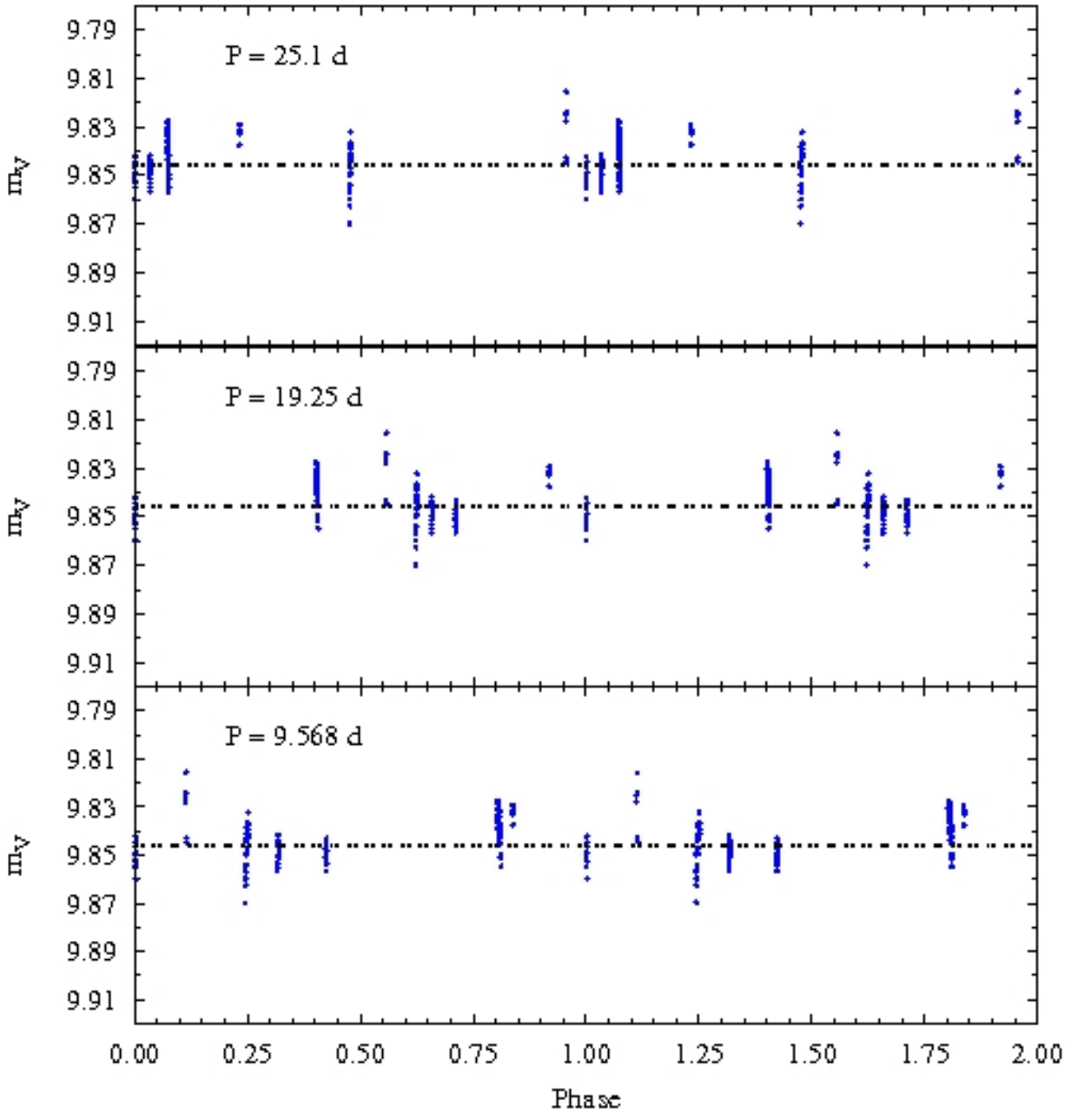

Figure 4.13 2010 data phased with the 9.6 d, 19.2 d, and 25.1 d periods

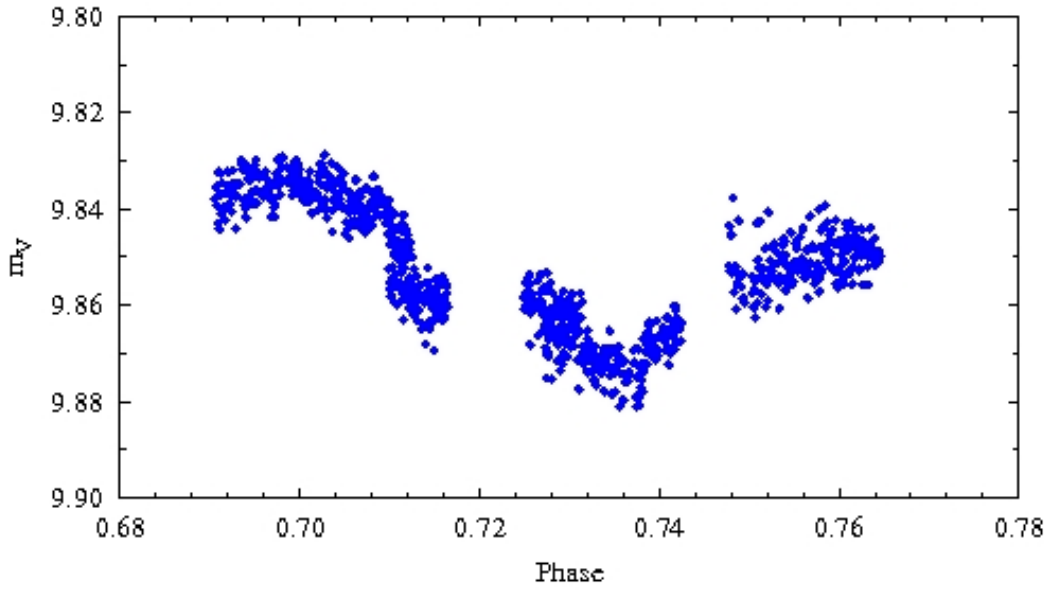

Figure 4.14 A zoomed in look at a few nights from 2008, phased with the 9.6 d period

4.1.1 Error Analysis

The errors per observation for 4U 2206+54 were relatively low for both telescopes in 2009 and 2010. Stars that did show high errors were removed from the distribution in *varstar*. The 2009 and 2010 data were plotted with error bars for each night in each filter, as illustrated in Figures 4.15 and 4.16. The size of the error bar represents the average error observation for that specific night and filter.

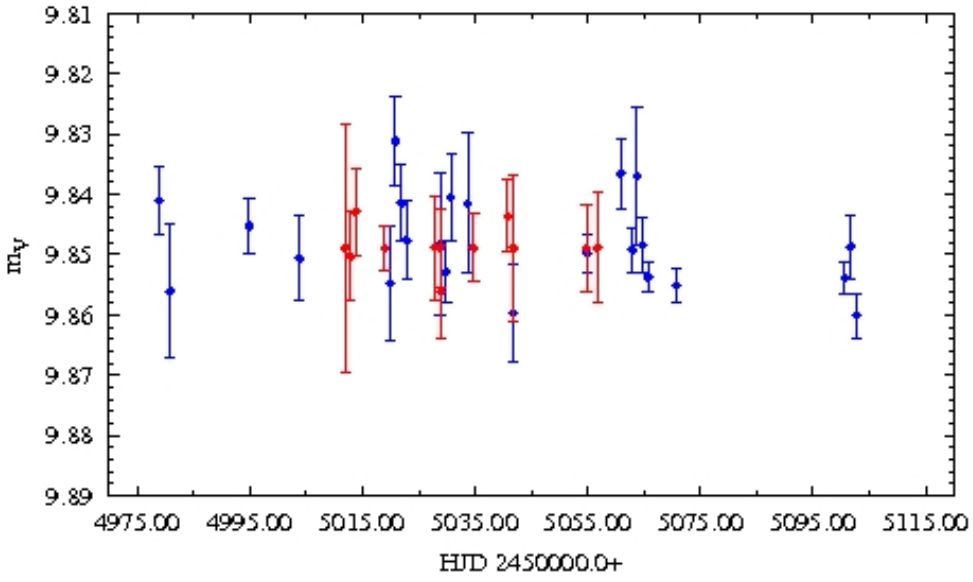

Figure 4.15 This plot shows the average error per observation of 4U 2206+54 for 2009 individual nights. OPO observations are blue, and WMO observations are red.

For a list of the average error per observation over a year for 4U 2206+54, see Table 4.1.

Table 4.1. Average Error per Observation for 4U 2206+54

Year	Observatory	Filter	Error
2010	WMO	B	0.0061
2010	WMO	V	0.0053
2010	WMO	R	0.0078*
2010	WMO	I	0.0058
2010	OPO	B	0.0087
2010	OPO	V	0.0050
2010	OPO	I	0.0058
2009	WMO	V	0.0071
2009	OPO	V	0.0063

Note. — The error listed for 2010 WMO in the *R* filter does not include the three nights that were overexposed.

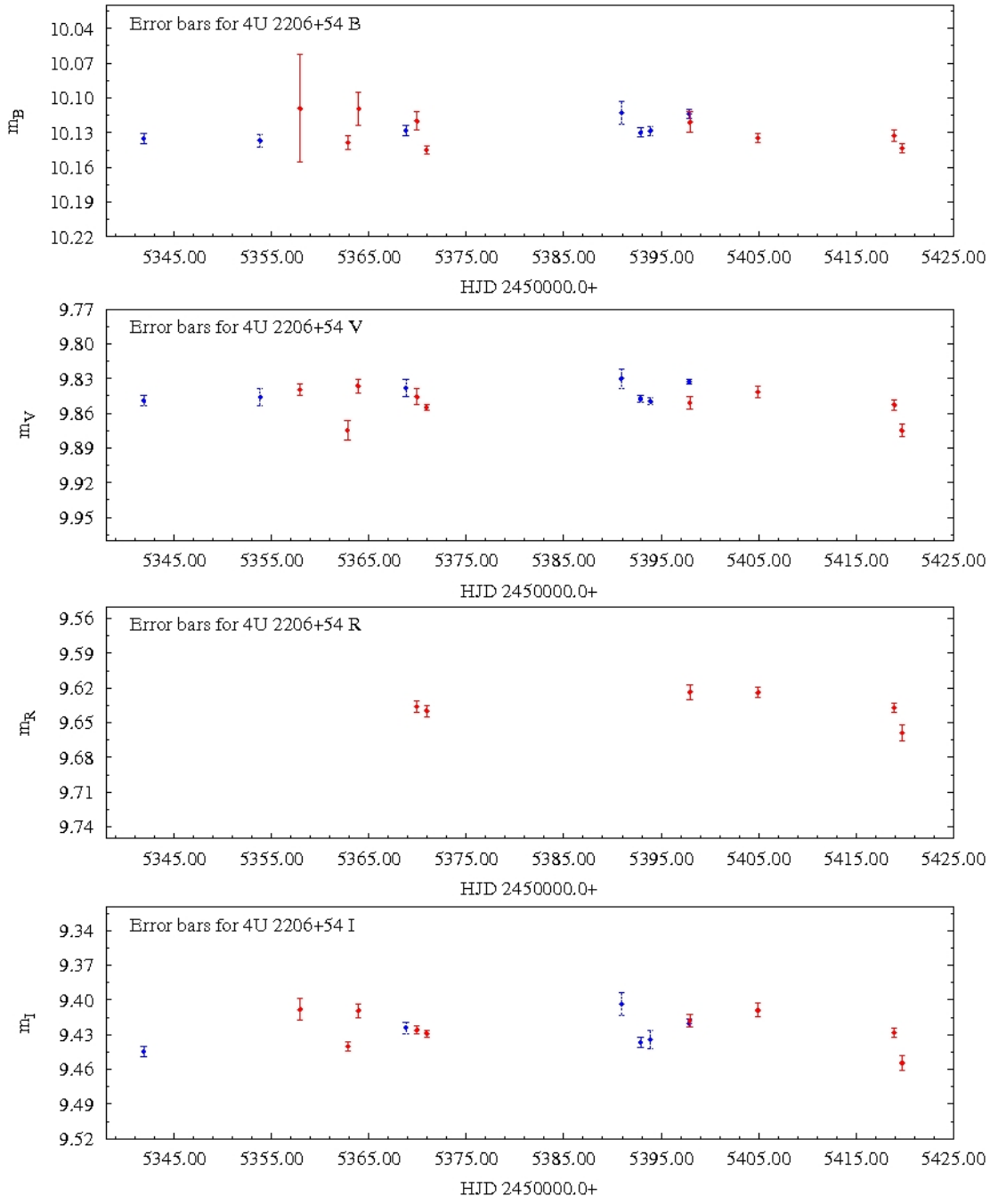

Figure 4.16 This plot shows the average error per observation of 4U 2206+54 in multiple filters for 2010 individual nights. OPO observations are blue, and WMO observations are red.

4.2 Spectroscopic Results

Besides the photometric data, spectral data was necessary to determine the spectral type of BD +53°2790. For this, we used data from Blay et al. (2005) and Blay et al. (2006), as well as received our own time at DAO from 2009 and 2010.

4.2.1 DAO

The spectral images from DAO were taken with a wide enough wavelength range such that both the $H\alpha$ and $H\beta$ lines were detected, as shown in Figure 4.17. For comparison, spectra covering

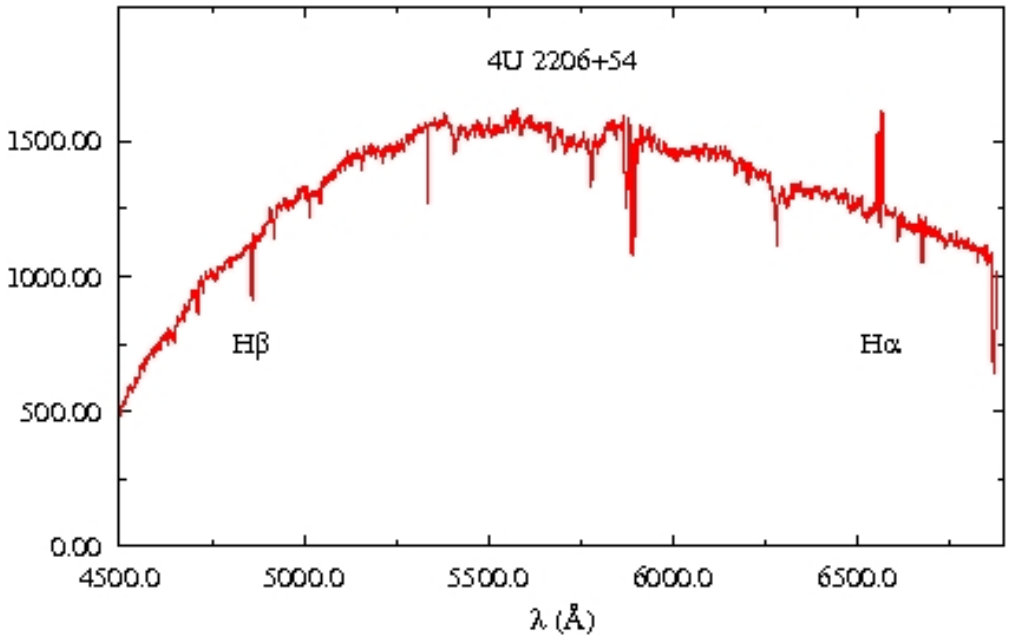

Figure 4.17 Our DAO observations captured both the $H\alpha$ and $H\beta$ lines. This is a plot of a typical spectra image of 4U 2206+54 from September 22, 2010.

both the $H\alpha$ and the $H\beta$ lines for a typical O4V star and B2V star are displayed in Figures 4.18

and 4.19 respectively.

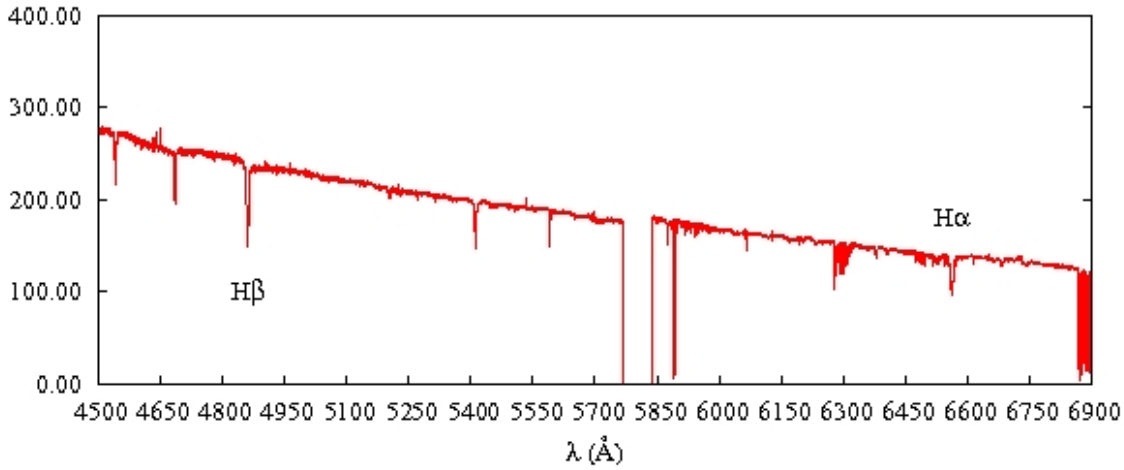

Figure 4.18 Spectrum of an O4V star covering both $H\alpha$ and $H\beta$ lines. Data were taken from http://www.sc.eso.org/santiago/uvespop/field_stars_uptonow.html

Our data show $H\alpha$ emission lines and $H\beta$ absorption lines. Similar to Blay et al. (2006), the $H\alpha$ lines were broken by an absorption trough as highlighted in Figure 4.20. At times, the peaks are equal in amplitude, but they have also been observed to be unequal by approximately 15%. This shifting suggests that different velocities are involved. This gives potential evidence for the theory that BD $+53°2790$ is actually a binary comprised of an O and B type star.

The constant profile of the $H\beta$ line implies that BD $+53°2790$ by itself is once again not the culprit for the noticeable variations because a stable profile suggests no change in temperature and size. Figure 4.21 shows the $H\beta$ profile for the same night as the $H\alpha$ profile. Therefore, it is likely that the changes we are seeing are due to the interaction between BD $+53°2790$ and its compact companion.

We were also able to compare 2009 spectra with 2010 spectra, as seen in Figures 4.22 and 4.23. All the frames on a given night were averaged to make a cleaner plot. In 2009, the $H\alpha$ trough goes

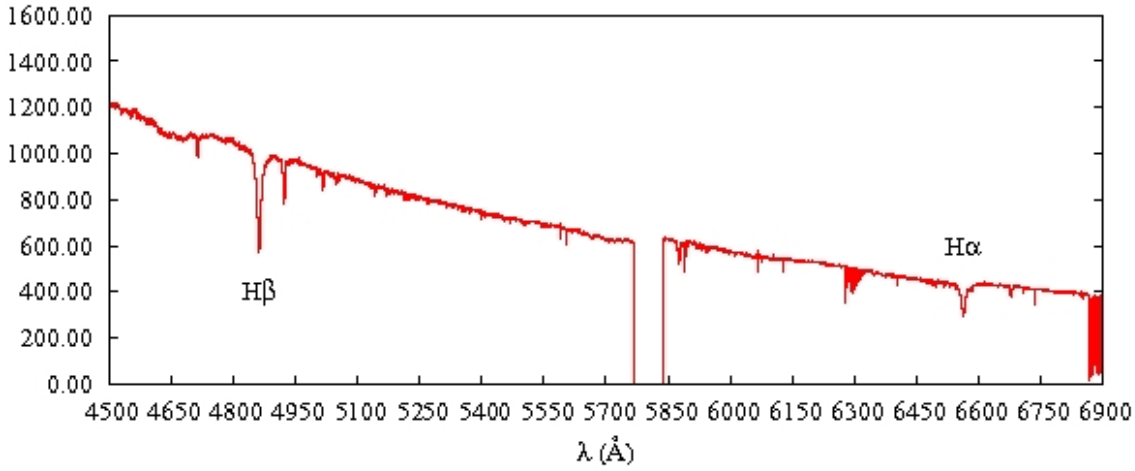

Figure 4.19 Spectrum of an B2V star covering both $H\alpha$ and $H\beta$ lines. Data were taken from http://www.sc.eso.org/santiago/uvespop/field_stars_uptonow.html

below the continuum. However, in 2010 that trough is noticeably shallower. $H\beta$ does remain fairly constant over this long term.

These nights of data were also compared to Blay's observations. 2009 data matched several nights, however, no period was determined due to gaps of no observations. 2010 data matched several nights in July 2000, but no previous Blay observations.

Another feature seen in our DAO spectra data, from approximately 5868 Å to 5905 Å, is highlighted in Figure 4.24. This feature is actually two lines, one emission (on the right) and one absorption (on the left). The emission line has been seen in all of the DAO data, as well as in other HMXBs. However, this emission line is not found in the spectra of O and B type stars. Further investigation identified this line as the Na I line at 5895 Å. It is telluric, which means it is due to the Earth's atmosphere. The absorption line has been identified as the He I line at 5875 Å. This is an important line to identify because it is significant to only some spectral types. A B0 star has the strongest He I line intensity, as displayed in Figure 1.2. The line in our data is not quite strong

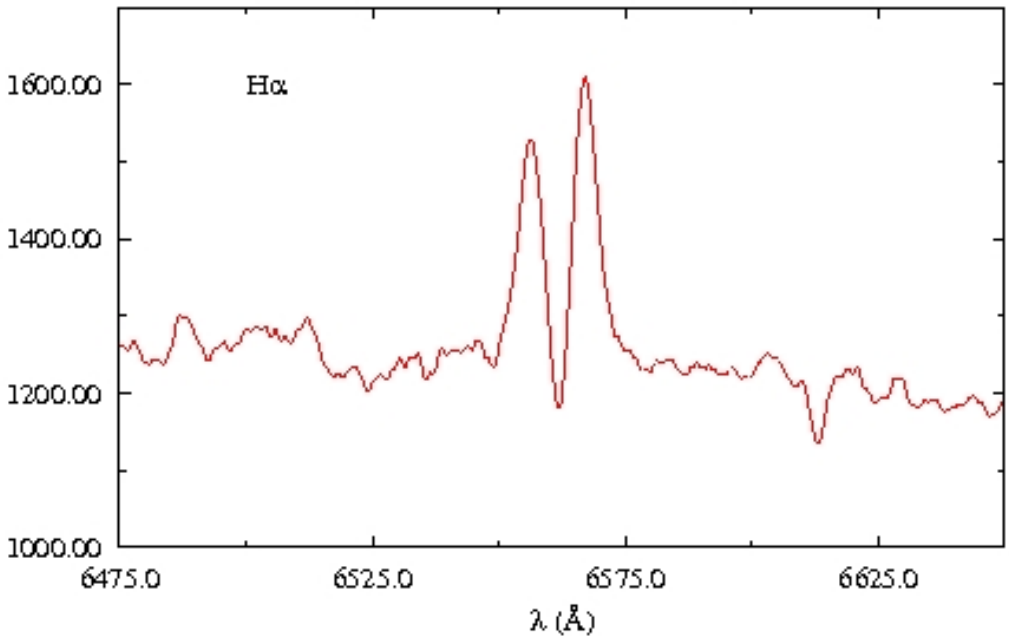

Figure 4.20 This is a spectral plot of 4U 2206+54 using DAO data from September 22, 2010, focusing on the $H\alpha$ line.

enough to be a B0 star, however, it does suggest that BD +53°2790 is either a late O or early B star. This line appears as absorption instead of emission because of the gas and dust shell. For more details about the gas and dust shell, see Sections 5.1 and 5.2.

4.2.2 Observatorio del Roque de los Muchachos

Spectral data results reported in Blay et al. (2006) from 1986 to 2000 showed $H\alpha$ emission, but with the peculiar trough in the center. It is noted that EW of $H\gamma$ remains constant throughout the observations. Changes in the temperature and radius of the primary star would cause the EW of a line to change. However, since there is no change, the variation in the $H\alpha$ line must be coming from something other than BD $+53°2790$. If the peculiar trough was in both $H\gamma$ and $H\alpha$, then the

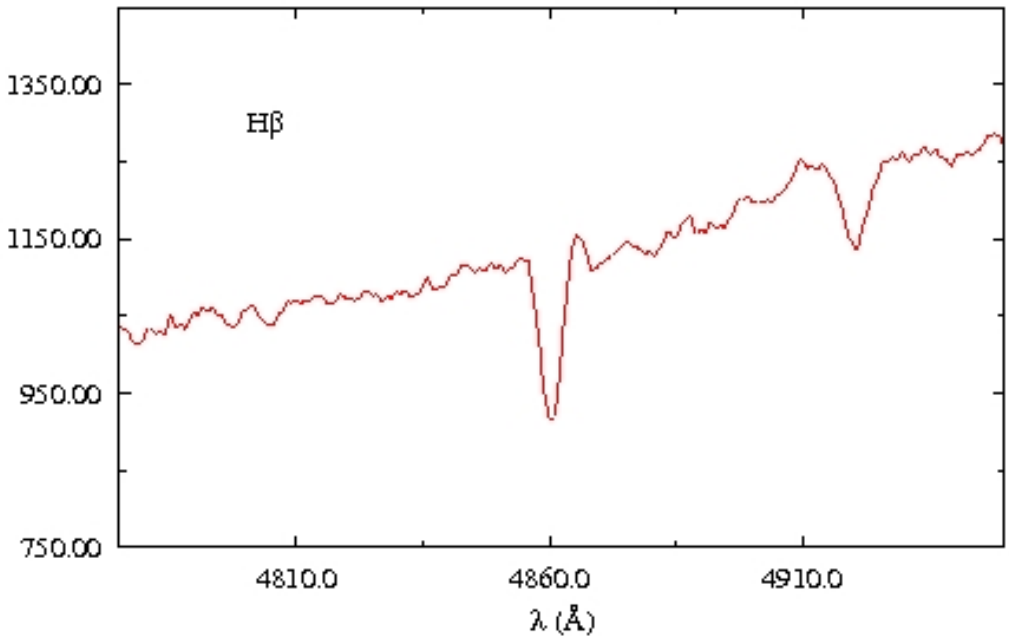

Figure 4.21 This is a spectral plot of 4U 2206+54 using DAO data from September 22, 2010, focusing on the $H\beta$ line.

variation would be caused by intrinsic features of the star. This, however, is not the case as seen in observations from not only Blay et al. (2006), but also from our own DAO data.

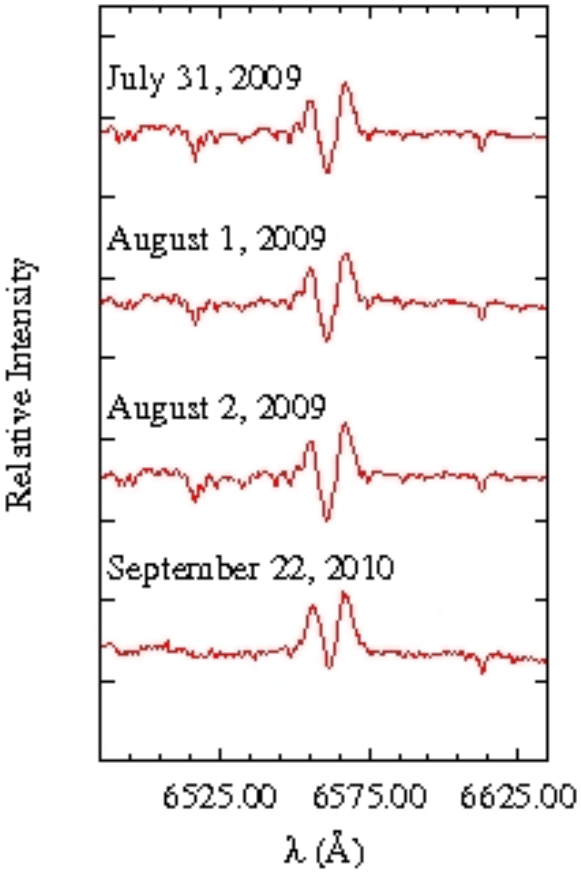

Figure 4.22 This plot shows multiple nights of $H\alpha$ observations in 2009, compared with one night from 2010.

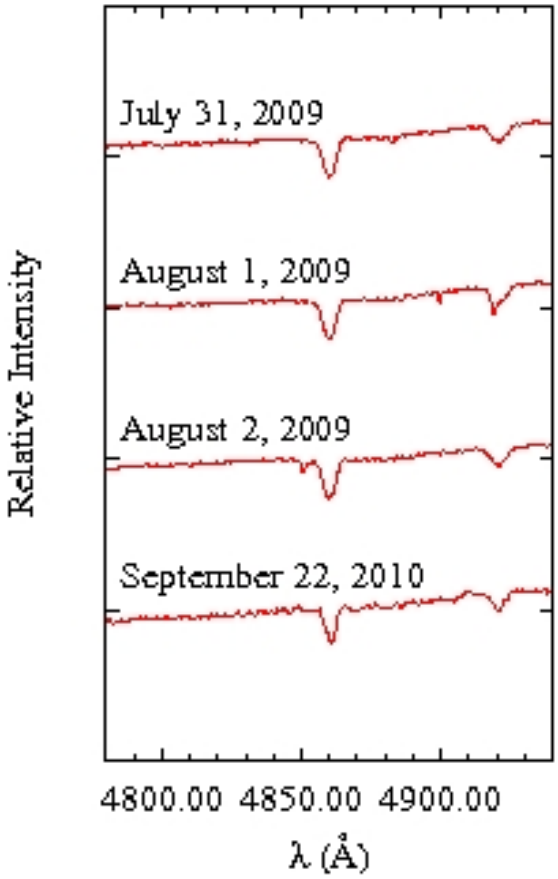

Figure 4.23 This plot shows multiple nights of $H\beta$ observations in 2009, compared with one night from 2010.

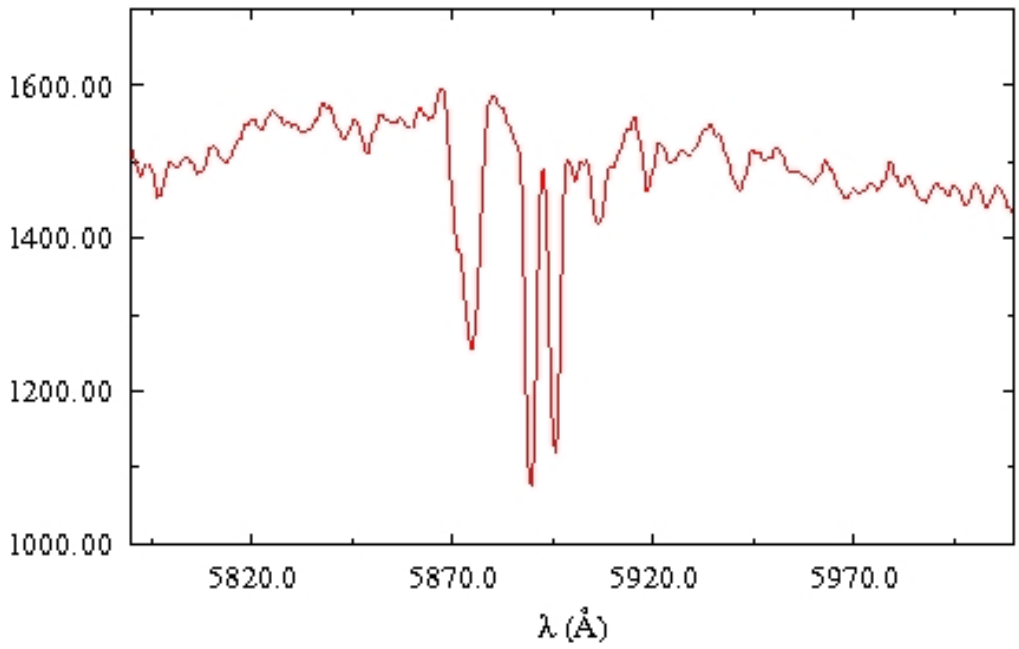

Figure 4.24 This is a spectral plot of 4U 2206+54 using DAO data from September 22, 2010, focusing on the telluric spectral feature.

Chapter 5

Discussion

5.1 Photometric Data

Photometric data for 4U 2206+54 were taken for three consecutive years using two different observatories. The 2008 data has shown a period of variability of 25.1 days. Using the program Period04 (Lenz & Breger 2005), a Fourier sine wave is fit to the data. The S/N for the 25.1 d period was 19.5. A S/N value of 5.0 is the lowest possible value that is acceptable, so for 2008, the 25.1 d period is significant. The S/N values for the 9.6 d period and 19.2 d period are 1.8 and 1.3 respectively. These values suggest that the two X-ray periods do not yield a good fit. The 2009 data does not visibly fit any of the three periods. This could be caused by unfortunate timing of observations, or that 4U 2206+54 was simply stable during this time. The 2010 data did not show such obvious variability as 2008 either, however, we do believe that some interaction is causing mild changes in source's magnitude. All three years of data were also loaded into Period04 to see if any periods fit over the long run. The most significant period detected was 30.99 days. The S/N for this fit was 5.01, which is just barely above the limit to be considered. However, taking into account that a respectable fit of 25.1 d produced a much higher S/N value, this long term period

does not seem significant.

Standardization of the field lead to a color value for 4U 2206+54. We found that $B-V=0.262$. This is unusual because main sequence O and B type stars have $B-V$ colors that are negative, meaning they are bluer, as listed in Table 1.1. This suggests that there may be a shell of gas and dust around 4U 2206+54 to give a redder color than expected.

5.2 Spectral Data

Spectra from 2010 were also analyzed, which once again showed the $H\alpha$ emission broken by a trough. One suggestion for this double-peaked feature is that two stars are being observed that have different velocities, which further supports the theory that BD +53°2790 is a binary instead of a single star. Even though the binary BD +53°2790 hypothesis explains the double-peaked $H\alpha$ line, it does not explain why the $H\beta$ line does not show the same feature.

There are several possible orientations for the double binary structure of 4U 2206+54. The three objects in this system are an O type star, a B type star, and the compact companion. One possibility is that the O and B stars are both orbiting the compact companion. This arrangement deconstructs into other configurations because it is unknown how far the O and B stars are from the compact companion. They could be approximately the same distance, or one star could be much farther away. A second structure is having the compact companion and either the O or B star in a binary, and then the other massive star orbits the system.

The observations from any of these structures can also be affected by the inclination angle of the system. It is possible we can see all three bodies at the same time. But it is also possible that we can only see one or two objects at a time. The strong and weak spectral lines from Negueruela & Reig (2001) suggest that we only observe one of the two massive stars at a time. Theoretically, it is possible that the O star and B star are eclipsing when only one strong set of spectral lines

is observed. However, photometric data indicate that an O and B star eclipse is not causing this pattern. If the two stars were observable at the same time, then when the eclipse happened, a substantial drop (several tenths of a magnitude) would occur due to losing visibility of such a bright star. This effect was not seen in the photometric data.

Another option for BD +53°2790 is a single star at the end of its main sequence lifetime. If the star began as a late O type star, the temperature would be hotter. As the star dies, it expands and begins to cool as it moves towards the red giant branch on the Hertzsprung-Russell diagram. At this point, BD +53°2790 would resemble an early B type star more than a late O star. As the star expands past the Roche lobe, matter is lost to the compact object. Eventually, enough matter is lost for the star to calm down and regain features of a late O star. While this theory explains the varying O and B star spectral lines, it does not explain the double-peaked feature of $H\alpha$.

A third option is that BD +53°2790 is a single star, but the unusual spectral features are due to a combination of the star and a gas and dust shell around the system. The gas in the shell could be glowing, which would give off emission lines. However, depending on the line of sight of the observer, absorption lines can been seen from the light of BD +53°2790 being absorbed by the shell. If the shell is circling around 4U 2206+54, then the $H\alpha$ emission line from the glowing shell will be slightly broadened. In this case, the line becomes broad enough that the $H\alpha$ absorption line is able to be seen in the middle of the emission, thus creating the double-peaked feature.

The issue of $H\alpha$ emission and $H\beta$ absorption must also be addressed. Normally, it would be expected to see both $H\alpha$ and $H\beta$ emission. However, in this particular case $H\beta$ is seen as absorption due to the gas and dust shell around 4U 2206+54. Photons that create the $H\beta$ emission line are bluer than the photons that create $H\alpha$, and bluer light will be more easily scattered by the dust and gas shell. $H\beta$ could have emission, but this is being washed out by so much absorption from the shell. Therefore, $H\beta$ would be an absorption line, and also not show the double-peaked feature.

A β Cepheid star is another explanation for the nature of BD +53°2790. It is also known that some β Cepheid variable stars have this peculiar trough feature. Since β Cepheids lie high on the main sequence, they are typically O and B type stars, which is the spectral classification range for BD $+53°2790$. However, a β Cepheid stars should also show periodic changes in brightness, that are not seen in the 2009 photometric data.

Chapter 6

Conclusions

6.1 4U 2206+54

Originally, it seemed like a binary BD $+53°2790$ comprised of an O-type star and a B-type star was the best fit for the data. While this idea explained the double-peaked $H\alpha$ feature seen in both spectra from Blay and DAO, it did not fit the photometric observations. An eclipse of the O and B star would certainly be noticeable, but was not detected. In addition, this theory does not explain why $H\alpha$ is seen as emission and $H\beta$ is absorption. Based on the spectra data and standardization of the photometric data, it is likely that there is a gas and dust shell around 4U 2206+54. Therefore, BD $+53°2790$ is just a single star contained in this shell. This design explains the double-peaked $H\alpha$ feature, as well as why $H\alpha$ is emission and $H\beta$ is absorption. The other possibilities for BD $+53°2790$ are not able to account for both characteristics.

The three orbital periods for 4U 2206+54 are 9.6 d, 19.2 d, and 25.1 d. The photometric data provide the clearest orbital period of 25.1 d. The two X-ray orbital periods were not significant based on the results of phasing the data, as well as S/N values determined by Period04.

6.2 Future Plans

6.2.1 Optical Observations

We still want to continue monitoring 4U 2206+54 in multiple filters using both WMO and OPO. It is possible that variation was undetected because of weather conditions and gaps in the data. Furthermore, it is probable that light variation of 4U 2206+54 will persist in the future. Because the variability of 2008 photometric data was not seen in the two following years, 4U 2206+54 will need to be studied for several more years to see if the 2008 pattern repeats.

Besides 4U 2206+54, there are several other interesting targets which we wish to observe more thoroughly, which are listed in Table 6.1. IGR J00370+6122 does not have an object type, but it seems relatively normal. This may act as a good comparison for 4U 2206+54 because it has a similar visual apparent magnitude.

XTE J0421+560 is interesting because it has high recorded magnitudes for the J, H, K filters in NIR. It is also one of the brightest HMXB sources in radio.

IGR J19140+0951, whose object type is unknown, is missing a value for apparent magnitude. In addition, this source was discovered in X-rays, as was 4U 2206+54. IGR J19140+0951 may also be a good comparison source for 4U 2206+54 because these two HMXBs have similar IR magnitudes.

IH 2202+501 is a third source not given an object type. It is not very strong in radio, and was discovered in optical. This source may also act as a basic comparison for 4U 2206+54.

The last secondary target is RX J0440.9+4431. It is a P type, meaning X-ray pulsar, and seems fairly ordinary.

Even though there are interesting characteristics for each of these targets, the most perplexing target is XTE J0421+560 due to unusually high radio and IR magnitudes that none of the other targets have. Because of this, we would like to focus on this target more than the other secondary

Table 6.1. Other Targets

Name	Type	RA (h:m:s)	Dec (d:m:s)	Visual Mag	Jmag	Hmag	Kmag	mJ
IGR J00370 + 6122	···	00 37 10.00	61 21 35.0	9.65	8.389	8.265	8.166	8
XTE J0421 + 560	T, R	04 19 42.20	55 59 59.0	9.25	7.502	5.741	4.323	2000
IGR J19140 + 0951	···	19 14 04.20	09 52 58.3	···	9.366	9.238	9.068	1.1
IH 2202 + 501	···	22 01 38.20	50 10 05.0	8.8	9.218	9.116	9.038	16
RX J0440.9 + 4431	P	04 40 59.30	44 31 49.0	10.78	9.5	9.317	9.182	1

Note. — T - Transient X-ray source, R - Radio emitting, P - X-ray pulsar

References. — Liu et al. (2006)

sources. We want to further investigate the high values in the NIR and radio wavelengths.

6.2.2 IR Observations

Because it is likely that there is a gas and dust shell around 4U 2206+54, IR observations of the target become very important. These observations can alleviate much of the confusion about the system's $B-V$ color value and also the dynamics of the spectral lines.

6.2.3 Radio Observations

We had intentions to schedule time at the Very Large Array (VLA) for observations of 4U 2206+54. Unfortunately, two different proposals were submitted, but both were denied. We do plan to once again request time for radio data in the future.

One reason for making observations in different wavelengths other than optical is so we can compare what is happening in a different part of the spectrum to get a better understanding of the physical processes taking place. It is possible that the optical and X-ray observations are detecting events that are not due to orbital motion. Radio observations can detect events such as emission

from the accretion disk on the neutron star, which do not have to be caused from orbital motion. In most cases, the high energy phenomena are followed by strong emission at low frequencies. The radio emission can be produced by the transfer of matter, similar to the X-rays.

In addition, radio observations can provide information on the power spectrum of the source. Not only would this show how the amplitude of the signal varies with wavelength, but it is also useful to identify what type of radiation process is at work. Such examples are Bremsstrahlung, synchrotron, etc.

Depending on the inclination of 4U 2206+54, a varying radio light curve can provide periodicity. If the same variation is seen in the optical lightcurves as seen in radio, that variation must be caused by the orbital motion. If the radio data shows a constant light curve, then when the neutron star passes in front of the O-type star, radio emission would not drop because we can still see the accretion disk. However, the optical data would show a drop because the O-type star is being blocked. If the inclination angle is not 0°, then when the neutron star travels farther away relative to the observer, we will still detect an accretion disk. In this case, a constant radio light curve would match a constant optical light curve.

Another aspect of this system that observations in radio might help us determine is the type of binary, either long or short period. If it is a short period binary, the continuous transfer of matter will be reflected in continuous radiation, whereas for the long period case, the emission would be sporadic. If we can detect continual transfer, then we will know that 4U 2206+54 is a short period HMXB. Once the type is determined, it is possible to narrow down the range of orbital periods.

There are several HMXBs that have been strong in radio wavelengths, such as LS 5039, SS 433, Cygnus X-1, and LSI+61°303 (Martí et al. 1998). LS 5039 was detected in L-band with a flux of approximately 24 mJy/beam. The most likely mechanism for the strong radio emission of this system was synchrotron radiation (Ribó et al. 1999). Study of LS 5039 is useful because it is very similar to 4U 2206+54. Both systems are believed to have either a neutron star or a black

hole for the compact companion. In the case of LS 5039, there has been detection of accretion on the compact companion due to the stellar winds of the massive star, which may also be the case in 4U 2206+54 (Ribó et al. 1999). In addition, according to Blay et al. (2006), BD $+53^{\circ}2790$ most likely contains an O9.5V star. Similarly, the high mass star of LS 5039 is an O7V star. This resemblance may produce comparable results in radio. Furthermore, 4U 2206+54 has already been observed using the VLA in the X-band. Unfortunately the data taken by Marc Ribó in those previous observations were not useful for our project due to spread out observations and observations in a different radio band. Blay et al. (2005) obtained VLA observations of 4U 2206+54 conducted during May 2003, and provided and upper limit of 0.039 mJy/beam. Blay's observations were only taken for two hours spread over two days. This was not a long enough time frame to study 4U 2206+54 for our orbital period purposes.

Bibliography

Barth, A. J. et al., 2011, AAS Meeting # 217, Talk 310.08

Barthelmy, S. D. et al., 2005, Space Sci. Rev., 120:143-164

Blay, P., Ribó, M., Negueruela, I., Torrejón, J. M., Reig, P., Camero, A., Mirabel, I. F., & Reglero, V., 2005, A&A, 438:963-972

Blay, P., Negueruela, I., Reig, P., Coe, M. J., Corbet, R. H. D., Fabregat, J., & Tarasov, A. E., 2006, A&A, 446:1095-1105

Charles, P. A. & Seward F. D., 1995, “Exploring the X-ray Universe" (Cambridge University Press)

Corbet, R. H. D., Markwardt, C. B., & Tueller, J., 2007, ApJ, 655:458-465

Corbet, R. H. D. & Peele, A. G., 2001, ApJ, 562:936-942

Freedman, R. A., & Kauffman, W. J., 2008, “Universe" (W. H. Freeman and Company)

Hintz, E. G. 2010, private communication

Hintz, E. G., Bugno, J. L., & Joner, M. D., 2009, IBVS, 5891

Kippenhahn, R. & Weigert, A., 1990, “Stellar Structure and Evolution" (Springer-Verlag)

Landolt, A. U., 1992, AJ, 104:340-371

Lenz, P. & Breger, M., 2005, CoAst, 146:53-146

Levine, A. M., et al. 1996, ApJ, 469:L33-L36

Liu, Q. Z., van Paradijs, J., & van den Heuvel, E. P. J. 2006, A&A, 455:1165-1168

Martí, J., Parades, J. M., Ribó, M., 1998, A&A, 338:L71-L74

Mihalas, D. & Binney, J., 1981, “Galactic Astronomy: Structure and Kinematics" (W. H. Freeman and Company)

Negueruela, I. & Reig, P., 2001, A&A, 371:1056-1064

Reid, N., 2010, (http://www-int.stsci.edu/ inr/intrins.html)

Reig, P., Torrejón, J. M., Negueruela, I., Blay, P., Ribó, M., Wilms, J., 2009, A&A, 494:1073-1082

Ribó, M., Parades, J. M., & Martí, J., 1999, New Astronomy Reviews, 43:545-547

Ribó, M., Negueruela, I., Blay, P., Torrejón, J. M., Reig, P., 2006, A&A 449:687-698

Sarty, G. E., Kiss, L. L., Johnston, H. M., Huziak, R., & Wu, K., 2007, JAAVSO, 35:327-335

Steiner, J. E., Ferrara, A., Garcia, M., Patterson, J., Schwartz, D. A., Warwick, R. S., Watson, M. G., & McClintock, J. E., 1984, ApJ, 280:688-694